Smart Structures Systems, *Vol. 21, No. 4 (2018) 493-519*
DOI: https://doi.org/10.12989/sss.2018.21.4.493

Free vibration and static analysis of functionally graded skew magneto-electro-elastic plate

M.C. Kiran and S.C. Kattimani*

Department of mechanical engineering, National Institute of Technology Karnataka Surathkal, 575025, India

(Received June 28, 2017, Revised January 28. 2018, Accepted February 8, 2018)

Abstract. This article presents a finite element (FE) model to assess the free vibration and static response of a functionally graded skew magneto-electro-elastic (FGSMEE) plate. Through the thickness material grading of FGSMEE plate is achieved using power law distribution. The coupled constitutive equations along with the total potential energy approach are used to develop the FE model of FGSMEE plate. The transformation matrix is utilized in bringing out the element matrix corresponding to the global axis to a local axis along the skew edges to specify proper boundary conditions. The effect of skew angle on the natural frequency of an FGSMEE plate is analysed. Further, the study includes the evaluation of the static behavior of FGSMEE plate for various skew angles. The influence of skew angle on the primary quantities such as displacements, electric potential, and magnetic potential, and secondary quantities such as stresses, electric displacement and magnetic induction is studied in detail. In addition, the effect of power-law gradient, thickness ratio, boundary conditions and aspect ratio on the free vibration and static response characteristics of FGSMEE plate has been investigated.

Keywords: skew plates; functionally graded plates; magneto-electro-elastic plates; finite element; free vibration; static analysis

1. Introduction

The functionally graded [FG] material has been evolved with the technological advancements in fabricating a material with functional properties. This new class of material has attracted many researchers to assess their mechanical behavior through basic structures like the beam, plate and shells (Ray *et al.* 1992, Kondaiah *et al.* 2015, 2017, Jiang and Ding 2004, 2005, 2007, Wang and Ding 2007, Ray *et al.* 2001, Kiran and Kattimani 2017, 2018a).

The utilization of FG materials as structural components has steadily increased in aerospace, civil and mechanical application in recent years due to their high strength and excellent thermal resistant properties (Mortensen and Suresh 1995, Pompe *et al.* 2003, Miyamoto *et al.* 2013, Ebrahimi *et al.* 2009, Ebrahimi and Rastgoo 2009, 2011). The functionally graded magneto-electro-elastic [FGMEE] material is one such material with functional properties and exhibit coupled piezoelectric and magnetostrictive behavior. Boomgaard (1978) introduced magneto-electro-elastic (MEE) composite constituted by piezoelectric and magnetostrictive constituents. Such composites exhibit magneto-electric coupling in addition to the electro-elastic and magneto-elastic coupling found in their individual phases. The material characteristics of MEE composite exhibit a controlled response to external factors such as mechanical loads, electric fields, and magnetic fields. This unique ability of these materials facilitates larger scope for their application in sensing, actuating, and controlling devices. They mainly find their presence in critical aerospace and marine structures (Koma and Zimick 2003). In addition, sensitivity of these materials makes them most suitable for surface sensitive electronic probes, devices (Nan *et al.* 2008) and in many sensors and actuators (Zhang *et al.* 2014). Applications of multiferroic MEE composites are related to high-frequency devices such as filters and oscillators that could be tuned by magnetic field, and recently, electrically tuneable microwave applications such as filters, oscillators and phase shifters (Nan *et al.* 2008). Further, they are also used in stress monitoring and non destructive testing devices (Kurlyandskaya *et al.* 2009, Barandiaran *et al.* 2009). The possibility of coupling the different fields can be exploited in transducer application, structural health monitoring, vibration control, energy harvesting and other applications (Milazzo 2014a).

The composites made of MEE materials are extensively investigated to assess their free vibration characteristics and static behavior under various loading conditions (Buchanan 2004, Wang *et al.* 2003, Ramirez *et al.* 2006, Guan 2012, Bhangale and Ganesan 2005, Chen *et al.* 2014, Lage *et al.* 2004, Moita *et al.* 2009). Pan and his co-researchers (Pan 2001, Pan and Heyliger 2002, 2003, Pan and Han 2005) proposed various analytical solutions to evaluate the free vibration and static response of MEE plate. Millazo (2014a, b, 2016) established different methods to study the behavior of MEE plate subjected to large deflection and free vibration. Kattimani and Ray (2014a, b, 2015) attained effective control of nonlinear vibrations in MEE plates and shells using active constrained layered damping treatment. The scaled boundary FE method was implemented by Liu *et al.* (2016) to ascertain the higher order solutions for MEE

*Corresponding author, Assistant Professor
E-mail: sck@nitk.ac.in

ISSN: 1738-1584 (Print), 1738-1991 (Online)

plate composed of non-uniform material. Wakmanski and Pan (2016) evaluated free vibration of multilayered MEE plate with non-local effect using 3-D analytical solutions. Influence of imperfect interface and fibre distribution on MEE properties of fibre reinforced composites was evaluated by Almeyda *et al.* (2017).

The study of FG structures has attracted many researchers recently. Li *et al.* (2008) investigated the structural characteristics of an FG, transversely isotropic, MEE circular plate subjected to a uniform load. Wang *et al.* (2011) studied the static behavior of an FG MEE circular plate under axisymmetric bending. Ebrahimi *et al.* (2017) analysed the vibration characteristics of porous material FG-MEE plates resting on elastic foundation. The effect of guided wave propagation in infinite FG plate was investigated by Xiao *et al.* (2016) via Chebyshev spectral element method. Zhou and Zhu (2016) analysed the vibration and bending characteristics of multiferroic rectangular plates using third-order shear deformation theory. A three-dimensional exact solution was explored by Li *et al.* (2017) for the uniformly loaded MEE field with an elliptical crack in shear mode. Ebrahimi and Barati (2016) investigated the buckling behavior of piezoelectrically actuated FG-MEE nano plates under the influence of magnetic field. Static characteristic of multiphase MEE beams under thermal load is investigated by Vinyas and Kattimani (2017a, b). Free vibration and bi-axial buckling of MEE nanoplate resting on an elastic foundation are studied by Jamalpoor *et al.* (2017). Bagheri *et al.* (2017) studied the static behavior of FG MEE strip containing multiple moving cracks. Vibration analysis of multiphase MEE plate under the influence of harmonic forces is presented by Shooshtari and Razavi (2017). Ebrahimi and Dabaggh (2017) studied the flexural wave propagation responses in FG MEE nano plate. The geometrically nonlinear vibration of multiferroic plates and shells was investigated by Kattimani (2017). Chen *et al.* (2017) studied the wave propagation characteristics on multilayered MEE plate.

The effect of geometrical changes in terms of skew angle on the structural characteristics of various FG structures has been extensively investigated. Kiran *et al.* (2018b) studied the influence of porosity on free vibration and static characteristics of the skew-FGMEE plate. Free vibration of FG quadrilateral microplates in the thermal environment was studied by Shenas and Malekzadeh (2016). Ruan and Wang (2016) investigated the transverse vibrations of moving skew plates made of FG material. Adineh and Kadkhodayan (2017) carried out three-dimensional thermo-elastic analysis and also obtained dynamic response of a multi-directional FG skew plate on elastic foundation. Free vibration characteristics of FG-CNT reinforced composite skew plates were assessed by Kiani (2016). García-Macías *et al.* (2016) investigated the static and free vibration behavior of FG-CNT reinforced skew plates. Ardestani *et al.* (2017) developed isogeometric analysis to assess the effect of CNT orientation on the static and vibration response of CNT-reinforced skew composite plates. An analytical investigation of dynamic instability of FG skew plates under periodic axial compression was carried out by Kumar *et al.* (2017).

The extensive literature review suggests that much work has been carried out in assessing the structural behavior of multilayered and FG rectangular MEE plates. Further, literature suggests that the skew plates possess excellent structural characteristics over rectangular plates. To the best of authors' knowledge, no attempt has been previously made to assess the structural characteristics of FGSMEE plates. Hence, in the current article, it is intended to evaluate the influence of geometric changes introduced in terms of plate skewness on the free vibration and static behavior of the FGSMEE plate. A finite element formulation is developed incorporating the transformation of local skew coordinates on to the global plate coordinates.

The influence of skew angle on the natural frequencies of the FGSMEE plate has been effectively investigated. Further, the static behavior of FGSMEE plate is evaluated thoroughly in terms of primary and secondary structural parameters such as the displacements, electric potential, magnetic potential, stresses, electric displacement, and magnetic induction. In addition, the influence of material gradient index is also studied. Further, the effect of boundary conditions, thickness ratio, and aspect ratio on the structural behavior of the FGSMEE plates is thoroughly investigated.

2. Problem description and governing equation

A schematic diagram of an FGSMEE plate with a Cartesian coordinate system attached to the corner of the plate is shown in Fig. 1(a). The length, the width and the total thickness of the plate are a, b and h, respectively. The skew angle of the FGSMEE plate is α. Fig. 1(b) illustrates the top view of the FGSMEE plate. The two opposite boundaries are lines $y = 0$ and $y = b \cos \alpha$, and the two opposite skewed edges are defined by the lines $x = y \tan \alpha$ and $x = a + y \tan \alpha$. The material properties of the FGSMEE plate are assumed to vary across the thickness. The bottom surface of the plate is piezoelectric ($BaTiO_3$) and the top surface being magnetostrictive ($CoFe_2O_4$). The displacement components u, v and w along x-, y-, and z-direction at any point in the FGSMEE plate can be represented by

$$\begin{aligned} u(x,y,z,t) &= u_0(x,y,t) + z\ \theta_x(x,y,t) \\ v(x,y,z,t) &= v_0(x,y,t) + z\ \theta_y(x,y,t) \\ w(x,y,z,t) &= w_0(x,y,t) + z\ \theta_z(x,y,t) + z^2 \kappa_z(x,y,t) \end{aligned} \tag{1}$$

where u_0 and v_0 are the translational displacements at any point on the mid-plane of the plate along x- and y-directions while w_0 is the transverse displacement along z-direction at any point in the FGSMEE plate. θ_x denote the generalized rotation of the normal to the middle plane of the FGSMEE plate about the y-axis while θ_y denote the generalized rotation of the normal to the middle plane of the FGSMEE plate about the x-axis. θ_z and κ_z are the generalized rotational displacements for the FGSMEE plate with respect to the thickness coordinate.

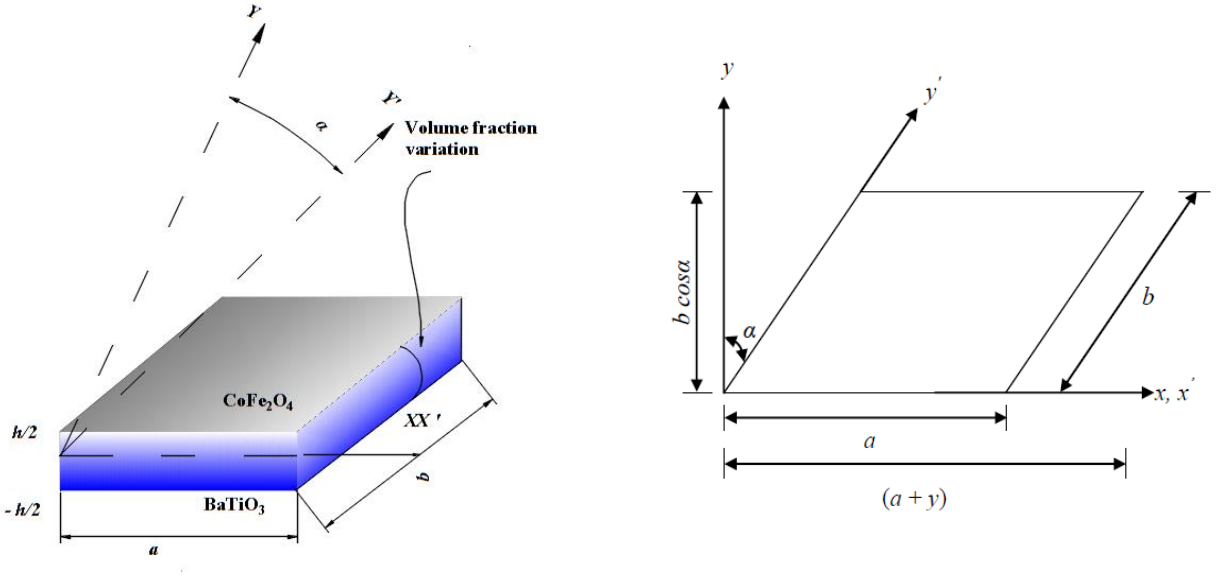

(a) (b)

Fig. 1 Schematic representation of (a) Functionally graded skew MEE plate. (b) Top view of FGSMEE plate

For the ease of computation, rotational and translational displacements are considered separately as follows

$$\{d_t\} = [u_0\ v_0\ w_0]^T,\ \{d_r\} = [\theta_x\ \theta_y\ \theta_z\ \kappa_z]^T \tag{2}$$

The selective integration rule is utilized to facilitate the computation of elemental stiffness matrices linked with the transverse shear deformation. This is achieved by separating the state of strain at any point in the plate by in-plane and transverse normal strain vector $\{\varepsilon_b\}$ and the transverse shear strain vector $\{\varepsilon_s\}$ as follows

$$\{\varepsilon_b\} = [\varepsilon_x\ \varepsilon_y\ \varepsilon_z\ \gamma_{xy}]^T,\ \{\varepsilon_s\} = [\gamma_{xz}\ \gamma_{yz}]^T \tag{3}$$

where, ε_x, ε_y and ε_z represent the normal strains along *x*-, *y*- and *z*-directions, respectively; γ_{xy} represents the in-plane shear strain, γ_{xz} and γ_{yz} are the transverse or out of plane shear strains. Making use of the displacement fields given in Eq. (1) and from the linear strain-displacement relations, the strain vectors $\{\varepsilon_b\}$ and $\{\varepsilon_s\}$ defining the state of inplane, transverse normal and transverse shear strain at any point in the FGSMEE plate can be expressed as

$$\{\varepsilon_b\} = \{\varepsilon_{bt}\} + [Z_1]\{\varepsilon_{br}\},\ \{\varepsilon_s\} = \{\varepsilon_{st}\} + [Z_2]\{\varepsilon_{sr}\} \tag{4}$$

wherein $\{\varepsilon_{bt}\}$ and $\{\varepsilon_{st}\}$ are the strain vectors corresponding to translation-bending and translation-rotation; $\{\varepsilon_{br}\}$ and $\{\varepsilon_{sr}\}$ are the strain vectors corresponding to rotational-bending and rotational-shear; the transformation matrices $[Z_1]$ and $[Z_2]$ are expressed as

$$[Z_1] = \begin{bmatrix} z & 0 & 0 & 0 & 0 \\ 0 & z & 0 & 0 & 0 \\ 0 & 0 & 0 & 1 & 2z \\ 0 & 0 & z & 0 & 0 \end{bmatrix},$$

$$[Z_2] = \begin{bmatrix} 1 & 0 & z & 0 & z^2 & 0 \\ 0 & 1 & 0 & z & 0 & z^2 \end{bmatrix}$$

The generalized strain vectors appearing in Eq. (4) are given by

$$\{\varepsilon_{bt}\} = \left[\frac{\partial u_0}{\partial x}\ \ \frac{\partial v_0}{\partial y}\ \ 0\ \ \frac{\partial u_0}{\partial y} + \frac{\partial v_0}{\partial x}\right]^T,$$

$$\{\varepsilon_{st}\} = \left[\frac{\partial w_0}{\partial x}\ \ \frac{\partial w_0}{\partial y}\right]^T,$$

$$\{\varepsilon_{br}\} = \left[\frac{\partial \theta_x}{\partial x}\ \ \frac{\partial \theta_y}{\partial y}\ \ \frac{\partial \theta_x}{\partial y} + \frac{\partial \theta_y}{\partial x}\ \ \theta_z\ \ \kappa_z\right]^T \text{ and}$$

$$\{\varepsilon_{sr}\} = \left[\theta_x\ \theta_y\ \frac{\partial \theta_z}{\partial x}\ \ \frac{\partial \theta_z}{\partial y}\ \ \frac{\partial \kappa_z}{\partial x}\ \ \frac{\partial \kappa_z}{\partial y}\right]^T$$

Analogous to the strain vectors given in Eq. (3), the state of stress at any point in the FGSMEE plate can be written as follows

$$\{\sigma_b\} = [\sigma_x\ \sigma_y\ \tau_{xy}\ \sigma_z]^T,\ \{\sigma_s\} = [\tau_{xz}\ \tau_{yz}]^T \tag{5}$$

in which, σ_x, σ_y and σ_z are the normal stresses along *x*-, *y*- and *z*-directions, respectively; τ_{xy} is the in-plane shear stress; τ_{xz} and τ_{yz} are the transverse shear stresses along

xz- and *yz*- directions, respectively. Considering the effect of coupled fields, the constitutive equations for the FGS MEE plate can be expressed as follows

$$\{\sigma_b\} = [C_b(z)]\{\varepsilon_b\} - \{e_b(z)\}E_z - \{q_b(z)\}H_z, \quad \{\sigma_s\} = [C_s(z)]\{\varepsilon_s\} \tag{6a}$$

$$D_z = \{e_b(z)\}^T\{\varepsilon_b\} + \xi_{33}(z)E_z + d_{33}(z)H_z \tag{6b}$$

$$B_z = \{q_b(z)\}^T\{\varepsilon_b\} + d_{33}(z)E_z + \mu_{33}(z)H_z \tag{6c}$$

where, $[C_b(z)]$ and $[C_s(z)]$ are the FG material coefficient matrices given as

$$[C_b(z)] = \begin{bmatrix} C_{11}(z) & C_{12}(z) & C_{13}(z) & C_{16}(z) \\ C_{12}(z) & C_{22}(z) & C_{23}(z) & C_{26}(z) \\ C_{13}(z) & C_{23}(z) & C_{33}(z) & C_{36}(z) \\ C_{16}(z) & C_{26}(z) & C_{36}(z) & C_{66}(z) \end{bmatrix}, \quad [C_s(z)] = \begin{bmatrix} C_{55}(z) & C_{45}(z) \\ C_{45}(z) & C_{44}(z) \end{bmatrix} \tag{7}$$

while, $\xi_{33}(z)$ and $\mu_{33}(z)$ are the dielectric constant and the magnetic permeability constant, respectively; $d_{33}(z)$ is the electromagnetic coefficient. The electric displacement, the electric field, the magnetic induction and the magnetic field along the *z*-direction are represented by D_z, E_z, B_z and H_z, respectively. The electric coefficient matrix $\{e_b(z)\}$ and the magnetic coefficient matrix $\{q_b(z)\}$ are given by

$$\{e_b(z)\} = \begin{Bmatrix} e_{31}(z) \\ e_{32}(z) \\ e_{33}(z) \\ e_{36}(z) \end{Bmatrix}, \quad \{q_b(z)\} = \begin{Bmatrix} q_{31}(z) \\ q_{32}(z) \\ q_{33}(z) \\ q_{36}(z) \end{Bmatrix} \tag{8}$$

The material properties are graded along the thickness direction of the plate by implementing the volume fraction power law distribution. The present study considers smooth and continuous variation of the constituent materials governed by power law gradient index. A simple power law for a functionally graded material can be assumed as (Kattimani and Ray 2015)

$$V = \left\{\left(\frac{z}{h}\right) + \left(\frac{1}{2}\right)\right\}^{\eta}$$

where, h is the thickness of the plate, z the thickness coordinate ($0 \le z \le h$), and η is the power law gradient index.

According to the definition of the volume fraction and rule of mixtures (Bhangale and Ganesan 2006), the various effective material properties can be written as follows

$$\bar{C}_{fg}(z) = C_F + (C_B - C_F)V, \quad \bar{\rho}_{fg}(z) = \rho_F + (\rho_B - \rho_F)V, \tag{9}$$

$$\bar{e}_{fg}(z) = e_F + (e_B - e_F)V, \quad \bar{q}_{fg}(z) = q_F + (q_B - q_F)V$$

$$\bar{\xi}_{fg}(z) = \xi_F + (\xi_B - \xi_F)V, \quad \bar{\mu}_{fg}(z) = \mu_F + (\mu_B - \mu_F)V$$

where, $\rho_{fg}(z)$ corresponds to the functionally graded material density. The subscript "*fg*" and the overlines stand for the effective material properties obtained by the above equations for a particular power law gradient index η. For the sake of brevity, the variation of functionally graded material properties in accordance with the variation in the power law gradient index is represented for elastic constant C_{11} alone for the sake of brevity in Fig.2.

Employing the principle of virtual work (Kattimani and Ray 2015), the governing equations for the FGSMEE plate is established as

$$\left(\int_{\Lambda}\delta\{\varepsilon_b\}^T\{\sigma_b\}d\Lambda + \int_{\Lambda}\delta\{\varepsilon_s\}^T\{\sigma_s\}d\Lambda + \int_{\Lambda}\delta\{d_t\}^T\rho(z)\{\ddot{d}_t\}d\Lambda\right) - \int_{\Lambda}\delta E_z D_z d\Lambda - \int_{\Lambda}\delta H_z B_z d\Lambda - \int_{A}\delta\{d_t\}^T F_t \, dA^{el} = 0 \tag{10}$$

where, Λ indicates the volume of the plate; A^{el} corresponds to the elemental surface area of the plate; F_t is the applied force with sinusoidal distribution on the top surface area A^{el} (Lage *et al*. 2004); ρ(z) denotes the mass density variation through the thickness. E_z and D_z are the electric fields and the electric displacements, respectively, while H_z and B_z are the magnetic fields and magnetic induction, respectively. The transverse electric field (E_z) related to the electric potential and the transverse magnetic field (H_z) is related to the magnetic potential in accordance with Maxwell's equation as follows (Kattimani and Ray 2015)

$$E_z = -\frac{\partial\phi}{\partial z} \quad \text{and} \quad H_z = -\frac{\partial\psi}{\partial z} \tag{11a}$$

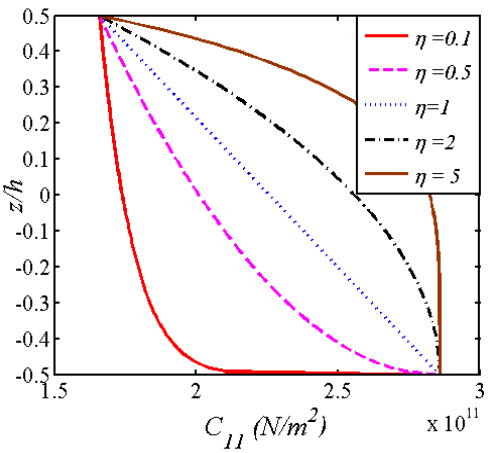

Fig. 2 Variation of C_{11} for different gradient index values η

where, ϕ and ψ are the electric and magnetic potential. It is noteworthy to mention that the thickness of FGSMEE plate is very small and hence, the variation of electric potential and magnetic potential functions can be assumed to be linear across the plate thickness.

Eq. (11(a)) can be rewritten as

$$E_z = -\frac{\partial}{\partial z}\{\phi\} \quad \text{and} \quad H_z = -\frac{\partial}{\partial z}\{\psi\} \tag{11b}$$

3. Finite element formulation

The FGSMEE plate is discretized using eight noded iso-parametric elements. Each node of the quadrilateral element has nine degree of freedom comprising of three translational DOF, three rotational DOF, one higher order rotation, one electrical, and one magnetic degree of freedom. In accordance with Eq. (3), the generalized displacement vectors $\{d_{ti}\}$ and $\{d_{ri}\}$ associated with the i^{th} node (where, i = 1, 2, 3, . . ., 8) of an element can be expressed as

$$\{d_{ti}\} = \begin{bmatrix} u_{0i} & v_{0i} & w_{0i} \end{bmatrix}^T \text{ and } \{d_{ri}\} = \begin{bmatrix} \theta_{xi} & \theta_{yi} & \theta_{zi} & \kappa_{zi} \end{bmatrix}^T \tag{12}$$

At any point within the element, the generalized displacement vectors $\{d_t\}$ and $\{d_r\}$, the magnetic potential vector $\{\psi\}$ and the electric potential vector $\{\phi\}$ can be expressed in terms of nodal generalized displacement vectors $\{d_t^{el}\}$ and $\{d_r^{el}\}$, the nodal magnetic potential vector $\{\psi^{el}\}$ and the nodal electric potential vector $\{\phi^{el}\}$, respectively, as follows

$$\begin{gathered} [d_t] = [N_t]\{d_t^{el}\}, \ \{d_r\} = [N_r]\{d_r^{el}\}, \\ \{\phi\} = [N_\phi]\{\phi^{el}\} \text{ and } \{\psi\} = [N_\psi]\{\psi^{el}\} \end{gathered} \tag{13}$$

in which

$$\begin{gathered} \{d_t^{el}\} = \left[\{d_{t1}^{el}\}^T \ \{d_{t2}^{el}\}^T \ldots \{d_{t8}^{el}\}^T \right]^T, \\ \{d_r^{el}\} = \left[\{d_{r1}^{el}\}^T \ \{d_{r2}^{el}\}^T \ldots \{d_{r8}^{el}\}^T \right]^T, \\ \{\phi^{el}\} = \{ \phi_1 \ \phi_2 \ \ldots \phi_8 \}^T, \\ \{\psi^{el}\} = \{ \psi_1 \ \psi_2 \ \ldots \psi_8 \}^T, \\ [N_t] = [N_{t1} \ N_{t2} \ \ldots \ N_{t8}]^T, \ [N_r] = [N_{r1} \ N_{r2} \ \ldots \ N_{r8}]^T, \\ [N_\phi] = [N_{\phi 1} \ N_{\phi 2} \ \ldots \ N_{\phi 8}]^T, \\ [N_\psi] = [N_{\psi 1} \ N_{\psi 2} \ \ldots \ N_{\psi 8}]^T \\ N_{ti} = n_i I_t, N_{ri} = n_i I_r \end{gathered} \tag{14}$$

where $[N_t]$, $[N_r]$, $[N_\phi]$ and $[N_\psi]$ corresponds to the shape function matrices, respectively and their expanded form is provided in Appendix. I_t and I_r are the identity matrices, respectively. n_i is the shape function of natural coordinate associated with the i^{th} node. ϕ_i (where, i = 1, 2, 3, . . ., 8) are the electric potential degrees of freedom and ψ_i are the magnetic potential degrees of freedom. Considering $\{\phi\}$ and $\{\psi\}$ from Eq. (13) and substituting in Eq. (11(b)), the transverse electric field (E_z) and the transverse magnetic field (H_z) are given by

$$E_z = -[b_\phi]\{\phi^{el}\} \quad \text{and} \quad H_z = -[b_\psi]\{\psi^{el}\} \tag{15}$$

where

$$[b_\phi] = \left[\frac{\partial N_{\phi i}}{\partial z} \right], \ [b_\psi] = \left[\frac{\partial N_{\psi i}}{\partial z} \right]$$

Now, using Eqs. (4) and (14), the generalized strain vectors at any point within the element can be expressed in 0.terms of the nodal generalized strain vectors as follows

$$\begin{gathered} \{\varepsilon_{bt}\} = [b_{tb}]\{d_t^{el}\} \ , \ \{\varepsilon_{br}\} = [b_{rb}]\{d_r^{el}\} \\ \{\varepsilon_{ts}\} = [b_{ts}]\{d_t^{el}\} \ , \ \{\varepsilon_{rs}\} = [b_{rs}]\{d_r^{el}\} \end{gathered} \tag{16}$$

in which, $[b_{tb}]$, $[b_{rb}]$, $[b_{ts}]$ and $[b_{rs}]$ are the nodal strain-displacement matrices and are provided in Appendix. Substituting Eqs. (4), (6), (14), (15) and (16) into Eq. (10) and simplifying, we obtain the elemental equations of motion for the FGSMEE plate as follows

$$\begin{gathered} [M^{el}]\{\ddot{d}_t^{el}\} + [k_{tt}^{el}]\{d_t^{el}\} + [k_{tr}^{el}]\{d_r^{el}\} + [k_{t\phi}^{el}]\{\phi^{el}\} \\ + [k_{t\psi}^{el}]\{\psi^{el}\} = \{F_t^{el}\} \end{gathered} \tag{17}$$

$$[k_{tr}^{el}]^T \{d_t^{el}\} + [k_{rr}^{el}]\{d_r^{el}\} + [k_{r\phi}^{el}]\{\phi^{el}\} + [k_{r\psi}^{el}]\{\psi^{el}\} = 0 \tag{18}$$

$$[k_{t\phi}^{el}]^T \{d_t^{el}\} + [k_{r\phi}^{el}]^T \{d_r^{el}\} - [k_{\phi\phi}^{el}]\{\phi^{el}\} = 0 \tag{19}$$

$$[k_{t\psi}^{el}]^T \{d_t^{el}\} + [k_{r\psi}^{el}]^T \{d_r^{el}\} - [k_{\psi\psi}^{el}]\{\psi^{el}\} = 0 \tag{20}$$

The matrices and the vectors appearing in Eqs. (17) - (20) are the elemental mass matrix $[M^{el}]$, the elemental elastic stiffness matrices $[k_{tt}^{el}]$, $[k_{tr}^{el}]$ and $[k_{rr}^{el}]$, the elemental electro-elastic coupling stiffness matrices and the elemental magneto-elastic coupling stiffness matrices are $[k_{t\phi}^{el}]$, $[k_{r\phi}^{el}]$ and $[k_{t\psi}^{el}]$, $[k_{r\psi}^{el}]$, respectively; $\{F_t^{el}\}$ is the elemental mechanical load vector; $[k_{\phi\phi}^{el}]$ and $[k_{\psi\psi}^{el}]$ are the elemental electric and elemental magnetic stiffness matrices, respectively. The stiffness matrices appearing in Eqs. (17) - (20) can be broadly classified correspondingly into mechanical, electrical, mechanical and couplings in Table 1.

The elemental matrices and vectors are given by

$$\left[k_{tt}^{el}\right]=\left[k_{tb}^{el}\right]+\left[k_{ts}^{el}\right],\ \left[k_{tr}^{el}\right]=\left[k_{trb}^{el}\right]+\left[k_{trs}^{el}\right],$$
$$\left[k_{rr}^{el}\right]=\left[k_{rrb}^{el}\right]+\left[k_{rrs}^{el}\right],\ \left[k_{t\phi}^{el}\right]=\left[k_{\phi t}^{el}\right]^{T},$$
$$\left[k_{t\psi}^{el}\right]=\left[k_{\psi t}^{el}\right]^{T},\left[k_{r\phi}^{el}\right]=\left[k_{\phi r}^{el}\right]^{T},\left[k_{r\psi}^{el}\right]=\left[k_{\psi r}^{el}\right]^{T}$$

where

$$\left[k_{tb}^{el}\right]=\int_0^{a_{el}}\int_0^{b_{el}}\left[b_{tb}\right]^T\left[D_{tb}\right]\left[b_{tb}\right]dx\,dy,$$
$$\left[k_{ts}^{el}\right]=\int_0^{a_{el}}\int_0^{b_{el}}\left[b_{ts}\right]^T\left[D_{ts}\right]\left[b_{ts}\right]dx\,dy$$
$$\left[k_{trb}^{el}\right]=\int_0^{a_{el}}\int_0^{b_{el}}\left[b_{tb}\right]^T\left[D_{trb}\right]\left[b_{rb}\right]dx\,dy,$$
$$\left[k_{trs}^{el}\right]=\int_0^{a_{el}}\int_0^{b_{el}}\left[b_{ts}\right]^T\left[D_{trs}\right]\left[b_{rs}\right]dx\,dy$$
$$\left[k_{rrb}^{el}\right]=\int_0^{a_{el}}\int_0^{b_{el}}\left[b_{rb}\right]^T\left[D_{rrb}\right]\left[b_{rb}\right]dx\,dy,$$
$$\left[k_{rrs}^{el}\right]=\int_0^{a_{el}}\int_0^{b_{el}}\left[b_{rs}\right]^T\left[D_{rrs}\right]\left[b_{rs}\right]dx\,dy$$
$$\left[k_{t\phi}^{el}\right]=\int_0^{a_{el}}\int_0^{b_{el}}\left[b_{tb}\right]^T\left[D_{t\phi}\right]\left[b_{\phi}\right]dx\,dy,$$
$$\left[k_{r\phi}^{el}\right]=\int_0^{a_{el}}\int_0^{b_{el}}\left[b_{rb}\right]^T\left[D_{r\phi}\right]\left[b_{\phi}\right]dx\,dy,$$
$$\left[k_{t\psi}^{el}\right]=\int_0^{a_{el}}\int_0^{b_{el}}\left[b_{tb}\right]^T\left[D_{t\psi}\right]\left[b_{\psi}\right]dx\,dy,$$
$$\left[k_{r\psi}^{el}\right]=\int_0^{a_{el}}\int_0^{b_{el}}\left[b_{rb}\right]^T\left[D_{r\psi}\right]\left[b_{\psi}\right]dx\,dy,$$
$$\left[k_{\phi\phi}^{el}\right]=\int_0^{a_{el}}\int_0^{b_{el}}\left[b_{\phi}\right]^T\left[D_{\phi\phi}\right]\left[b_{\phi}\right]dx\,dy,$$
$$\left[k_{\psi\psi}^{el}\right]=\int_0^{a_{el}}\int_0^{b_{el}}\left[b_{\psi}\right]^T\left[D_{\psi\psi}\right]\left[b_{\psi}\right]dx\,dy \quad (21)$$

where, a^{el} and b^{el} corresponds to the length and width of the element under consideration. $\left[D_{tb}\right]$, $\left[D_{ts}\right]$, $\left[D_{trb}\right]$, $\left[D_{trs}\right]$, $\left[D_{rrb}\right]$, $\left[D_{rrs}\right]$, $\left[D_{t\phi}\right]$, $\left[D_{r\phi}\right]$, $\left[D_{t\psi}\right]$, $\left[D_{r\psi}\right]$, $\left[D_{\phi\phi}\right]$ and $\left[D_{\psi\psi}\right]$ are the rigidity matrices appearing in Eq. (21) are given as follows

$$\left[D_{tb}\right]=\int_{-h/2}^{h/2}\left[C_b\right]dz,\ \left[D_{ts}\right]=\int_{-h/2}^{h/2}\left[C_s\right]dz,$$
$$\left[D_{trb}\right]=\int_{-h/2}^{h/2}\left[C_b\right]\left[Z_1\right]dz,\quad \left[D_{trs}\right]=\int_{-h/2}^{h/2}\left[C_s\right]\left[Z_2\right]dz \quad (22)$$
$$\left[D_{rrb}\right]=\int_{-h/2}^{h/2}\left[Z_1\right]^T\left[C_b\right]\left[Z_1\right]dz,$$
$$\left[D_{rrs}\right]=\int_{-h/2}^{h/2}\left[Z_2\right]^T\left[C_s\right]\left[Z_2\right]dz$$
$$\left[D_{t\phi}\right]=\int_{-h/2}^{h/2}\left\{e_b(z)\right\}\frac{1}{h}dz,\ \left[D_{t\psi}\right]=\int_{-h/2}^{h/2}\left\{q_b(z)\right\}\frac{1}{h}dz,$$
$$\left[D_{r\phi}\right]=\int_{-h/2}^{h/2}\left[z_1\right]^T\left\{e_b(z)\right\}\frac{1}{h}dz$$
$$\left[D_{r\psi}\right]=\int_{-h/2}^{h/2}\left[z_1\right]^T\left\{q_b(z)\right\}\frac{1}{h}dz$$
$$\left[D_{\phi\phi}\right]=\frac{\xi_{33}(z)}{h}\begin{bmatrix}1&0\\0&1\end{bmatrix},\ \left[D_{\psi\psi}\right]=\frac{1}{h}\mu_{33}(z)$$

3.1 Skew boundary transformation

In case of FG skew MEE plates, the supported adjacent edges of the boundary element are not parallel to the global axes (*x*, *y*, *z*). Hence, in order to specify the boundary conditions at the skew edges of the plate, the displacements *u'*, *v'* and *w'* at any point on the skew edges of the local coordinates must be restrained along the *x'*-, *y'*- and *z'*-directions. The boundary conditions can be specified conveniently by transforming the element matrices corresponding to the global axis to the local axis along the edges. A simple transformation relation can be expressed between the local degrees of freedom and the global degrees of freedom for the generalized displacement vectors of a point lying on the skew edges of the plate as follows

$$\left\{d_t\right\}=\left[L_t\right]\left\{d_t'\right\},\ \left\{d_r\right\}=\left[L_r\right]\left\{d_r'\right\}$$
$$\left\{d_t'\right\}=\left[u_0'\ v_0'\ w_0'\right]^T,\ \left\{d_r'\right\}=\left[\theta_x'\ \theta_y'\ \theta_z'\ \kappa_z'\right]^T \quad (23)$$

where, $\left\{d_t\right\}$, $\left\{d_r\right\}$ and $\left\{d_t'\right\}$, $\left\{d_r'\right\}$ are the displacements on the global and the local edge coordinate system, respectively. $\left[L_t\right]$ and $\left[L_r\right]$ are the transformation matrices for a node on the skew boundary and is given by

$$\left[L_t\right]=\begin{bmatrix}c&s&0\\-s&c&0\\0&0&1\end{bmatrix},\ \left[L_r\right]=\begin{bmatrix}c&s&0&0\\-s&c&0&0\\0&0&1&0\\0&0&0&1\end{bmatrix} \quad (24)$$

Table 1 Classification of stiffness matrix

Stiffness matrix	Coupling
$\left[k_{tt}^{el}\right]$, $\left[k_{tr}^{el}\right]$, $\left[k_{rr}^{el}\right]$	Mechanical
$\left[k_{\phi\phi}^{el}\right]$	Electric
$\left[k_{\psi\psi}^{el}\right]$	Magnetic
$\left[k_{t\phi}^{el}\right]$, $\left[k_{r\phi}^{el}\right]$	Electro-elastic coupling
$\left[k_{t\psi}^{el}\right]$, $\left[k_{r\psi}^{el}\right]$	Magneto-elastic coupling

in which, $c = cos\alpha$ and $s = sin\alpha$, the skew angle of the plate is α. It may be noted that for the nodes which does not lie on the skew edges, the transformation from global coordinates to the local coordinates is not required. The transformation matrices in such cases are the diagonal matrices in which the values of the principle diagonal elements are unity. Thus, considering Eq. (21), the elemental stiffness matrices of the element containing the nodes laying on the skew edges are given as follows

$$\left[\bar{k}_{tt}^{el}\right]=\left[T_1\right]^T\left[k_{tt}^{el}\right]\left[T_1\right],\ \left[\bar{k}_{tr}^{el}\right]=\left[T_1\right]^T\left[k_{tr}^{el}\right]\left[T_2\right]$$
$$\left[\bar{k}_{rr}^{el}\right]=\left[T_2\right]^T\left[k_{rr}^{el}\right]\left[T_2\right],\left[M^{el}\right]=\left[T_1\right]^T\left[M^{el}\right]\left[T_1\right] \tag{25}$$

where, the transformation matrices $[T_1]$ and $[T_2]$ are given by

$$\left[T_1\right]=\begin{bmatrix}\left[L_t\right]&\tilde{o}&\tilde{o}&\tilde{o}&\tilde{o}&\tilde{o}&\tilde{o}&\tilde{o}\\ \tilde{o}&\left[L_t\right]&\tilde{o}&\tilde{o}&\tilde{o}&\tilde{o}&\tilde{o}&\tilde{o}\\ \tilde{o}&\tilde{o}&\left[L_t\right]&\tilde{o}&\tilde{o}&\tilde{o}&\tilde{o}&\tilde{o}\\ \tilde{o}&\tilde{o}&\tilde{o}&\left[L_t\right]&\tilde{o}&\tilde{o}&\tilde{o}&\tilde{o}\\ \tilde{o}&\tilde{o}&\tilde{o}&\tilde{o}&\left[L_t\right]&\tilde{o}&\tilde{o}&\tilde{o}\\ \tilde{o}&\tilde{o}&\tilde{o}&\tilde{o}&\tilde{o}&\left[L_t\right]&\tilde{o}&\tilde{o}\\ \tilde{o}&\tilde{o}&\tilde{o}&\tilde{o}&\tilde{o}&\tilde{o}&\left[L_t\right]&\tilde{o}\\ \tilde{o}&\tilde{o}&\tilde{o}&\tilde{o}&\tilde{o}&\tilde{o}&\tilde{o}&\left[L_t\right]\end{bmatrix},$$
$$\left[T_2\right]=\begin{bmatrix}\left[L_r\right]&\breve{o}&\breve{o}&\breve{o}&\breve{o}&\breve{o}&\breve{o}&\breve{o}\\ \breve{o}&\left[L_r\right]&\breve{o}&\breve{o}&\breve{o}&\breve{o}&\breve{o}&\breve{o}\\ \breve{o}&\breve{o}&\left[L_r\right]&\breve{o}&\breve{o}&\breve{o}&\breve{o}&\breve{o}\\ \breve{o}&\breve{o}&\breve{o}&\left[L_r\right]&\breve{o}&\breve{o}&\breve{o}&\breve{o}\\ \breve{o}&\breve{o}&\breve{o}&\breve{o}&\left[L_r\right]&\breve{o}&\breve{o}&\breve{o}\\ \breve{o}&\breve{o}&\breve{o}&\breve{o}&\breve{o}&\left[L_r\right]&\breve{o}&\breve{o}\\ \breve{o}&\breve{o}&\breve{o}&\breve{o}&\breve{o}&\breve{o}&\left[L_r\right]&\breve{o}\\ \breve{o}&\breve{o}&\breve{o}&\breve{o}&\breve{o}&\breve{o}&\breve{o}&\left[L_r\right]\end{bmatrix} \tag{26}$$

in which, $\tilde{o}$ and $\breve{o}$ are the (3×3) and (5×5) null matrices, respectively and the number of $[L_t]$ and $[L_r]$ matrices are equal to the number of nodes in the element. The elemental equations of motion are assembled to obtain the global equations of motion of the FGSMEE plate as follows

$$\left[M\right]\left\{\ddot{d}_t\right\}+\left[k_{tt}^g\right]\left\{d_t\right\}+\left[k_{tr}^g\right]\left\{d_r\right\}+\left[k_{t\phi}^g\right]\left\{\phi\right\}+\left[k_{t\psi}^g\right]\left\{\psi\right\}=\left\{F_t\right\} \tag{27}$$

$$\left[k_{tr}^g\right]^T\left\{d_t\right\}+\left[k_{rr}^g\right]\left\{d_r\right\}+\left\{k_{r\phi}^g\right\}\left\{\phi\right\}+\left[k_{r\psi}^g\right]\left\{\psi\right\}=0 \tag{28}$$

$$\left[k_{t\phi}^g\right]^T\left\{d_t\right\}+\left[k_{r\phi}^g\right]^T\left\{d_r\right\}-\left[k_{\phi\phi}^g\right]\left\{\phi\right\}=0 \tag{29}$$

$$\left[k_{t\psi}^g\right]^T\left\{d_t\right\}+\left[k_{r\psi}^g\right]^T\left\{d_r\right\}-\left[k_{\psi\psi}^g\right]\left\{\psi\right\}=0 \tag{30}$$

where, $[M]$ is the global mass matrix; $\left[k_{tt}^g\right]$, $\left[k_{tr}^g\right]$ and $\left[k_{rr}^g\right]$ are the global elastic stiffness matrices; $\left[k_{t\phi}^g\right]$ and $\left[k_{r\phi}^g\right]$ are the global electro-elastic coupling stiffness matrices; $\left[k_{t\psi}^g\right]$ and $\left[k_{r\psi}^g\right]$ are the global magneto-elastic coupling stiffness matrices; $\{F_t\}$ is the global mechanical load vector; $\left[k_{\phi\phi}^g\right]$ and $\left[k_{\psi\psi}^g\right]$ are the global electric and the global magnetic stiffness matrices, respectively. Solving the global equations of motion (Eqs. (28)-(30)) to obtain global generalized displacement vector $\{d_t\}$ and $\{d_r\}$ by condensing the global degrees of freedom for $\{\phi\}$ and $\{\psi\}$ in terms of $\{d_r\}$ as follows

$$\left\{\psi\right\}=\left\{k_{\psi\psi}^g\right\}^{-1}\left[k_{t\psi}^g\right]^T d_t+\left[k_{\psi\psi}^g\right]^{-1}\left[k_{r\psi}^g\right]^T\left\{d_r\right\},$$
$$\left\{\phi\right\}=\left[k_{\phi\phi}^g\right]^{-1}\left[k_{t\phi}^g\right]^T\left\{d_t\right\}+\left[k_{\phi\phi}^g\right]^{-1}\left[k_{r\phi}^g\right]^T\left\{d_r\right\}, \tag{31}$$
$$\left\{d_r\right\}=-\left[K_3\right]^{-1}\left[K_2\right]^T\left\{d_t\right\}$$

Now, substituting Eq. (31) in Eq. (27) and upon simplification, we obtain the global equations of motion in terms of the global translational degrees of freedom as follows

$$\left[M\right]\left\{\ddot{d}_t\right\}+\left[K\right]\left\{d_t\right\}=\left\{F_t\right\}$$
$$\text{and } \left[K\right]=\left(\left[K_1\right]-\left[K_2\right]\left[K_3\right]^{-1}\left[K_2\right]^T\right) \tag{32}$$

where, the global assembled matrices are given as follows

$$\left[K_1\right]=\left[k_{tt}^g\right]+\left[k_{t\phi}^g\right]\left[k_{\phi\phi}^g\right]^{-1}\left[k_{t\phi}^g\right]^T+\left[k_{t\psi}^g\right]\left[k_{\psi\psi}^g\right]^{-1}\left[k_{t\psi}^g\right]^T$$
$$\left[K_2\right]=\left[k_{tr}^g\right]+\left[k_{t\phi}^g\right]\left[k_{\phi\phi}^g\right]^{-1}\left[k_{r\phi}^g\right]^T+\left[k_{t\psi}^g\right]\left[k_{\psi\psi}^g\right]^{-1}\left[k_{r\psi}^g\right]^T$$
$$\left[K_3\right]=\left[k_{rr}^g\right]+\left[k_{r\phi}^g\right]\left[k_{\phi\phi}^g\right]^{-1}\left[k_{r\phi}^g\right]^T+\left[k_{r\psi}^g\right]\left[k_{\psi\psi}^g\right]^{-1}\left[k_{r\psi}^g\right]^T$$

4. Results and discussion

This section involves the validation of present FE formulation and to ascertain new results corresponding to the free vibration and static behavior of FGSMEE plate. The material properties used in the present analysis are given in Table 2 (Kattimani and Ray 2015). The non-homogeneous transversely isotropic FGSMEE plate is functionally graded along the thickness by implementing the power law (Kattimani and Ray 2015). For all the values of power law index (except for pure magnetostrictive and pure piezoelectric plate i.e., η = 0 and η = ∞) different variation of material properties in between the bottom piezoelectric and the top magnetostrictive plate is achieved. The value of the shear correction factor is used as 5/6. Three point Gaussian integration rule are considered for computing the element matrices corresponding to bending deformation while two points of that are used for computing the element matrices corresponding to transverse shear deformation. The boundary conditions involved in the present analysis are given as follows:

(a) Simply supported edges

at $x = y\tan\alpha$, $x = a + y\tan\alpha$:

$$v_0^1 = w_0^1 = \theta_y^1 = \theta_z^1 = \phi^1 = \psi^1 = 0$$

at $y = 0$, $y = b\cos\alpha$: (33)

$$\text{(a)}\quad u_0 = w_0 = \theta_z = \phi = \psi = 0$$

(b) Clamped edges

at $x = y\tan\alpha$, $x = a + y\tan\alpha$:

$$u_0^1 = v_0^1 = w_0^1 = \theta_x^1 = \theta_y^1 = \theta_z^1 = \phi^1 = \psi^1 = 0$$

at $y = 0$, $y = b\cos\alpha$: (34)

$$u_0 = v_0 = w_0 = \theta_x = \theta_y = \theta_z = \phi = \psi = 0$$

(c) Free edges

at $x = y\tan\alpha$, $x = a + y\tan\alpha$:

$$u_0^1 = v_0^1 = w_0^1 = \theta_x^1 = \theta_y^1 = \theta_z^1 = \phi^1 = \psi^1 \neq 0$$

at $y = 0$, $y = b\cos\alpha$: (35)

$$u_0 = v_0 = w_0 = \theta_x = \theta_y = \theta_z = \phi = \psi \neq 0$$

where, ϕ and ψ are the electric and magnetic potential degrees of freedom, respectively, as specified in the previous section.

4.1 Validation studies

The correctness of the FE model proposed in the previous section is verified against some of the available studies in literature. The free vibration study of FGMEE plate proposed by Milazzo (2014a) is considered for the validation. The natural frequencies for the simply supported FGMEE having the material gradient index, η = 1, aspect ratio of b/a = 2 and thickness ratio of h/a = 0.1 and 0.2 is presented in Table 3. The convergence study is also presented in Table 3. It can be seen from the tabulated results that for a 20 × 20 mesh size, an excellent agreement is achieved with the solutions available in literature.

Table 2 Material properties of $BaTiO_3$ and $CoFe_2O_4$ (Kattimani and Ray 2015)

Material properties	$BaTiO_3$	$CoFe_2O_4$
$C_{11} = C_{22}$ (10^9 N/m^2)	166	286
C_{12} (10^9 N/m^2)	77	173
$C_{13} = C_{23}$ (10^9 N/m^2)	78	170.5
C_{33} (10^9 N/m^2)	162	269.5
$C_{44} = C_{55}$ (10^9 N/m^2)	43	45.3
C_{66} (10^9 N/m^2)	44.5	56.5
ρ (kg/m^3)	5300	5800
$e_{31} = e_{32}$ (C/m^2)	- 4.4	-
e_{33} (C/m^2)	18.6	-
$\xi_{11} = \xi_{22}$ (10^{-9} C/Nm^2)	11.2	0.08
$\mu_{11} = \mu_{22}$ (10^{-6} Ns^2/C^2)	5	- 590
μ_{33} (10^{-6} Ns^2/C^2)	10	157
$q_{31} = q_{32}$ (N/Am)	-	180.3
q_{33} (N/Am)	-	699.7

Therefore, for all the subsequent analysis, a mesh size of 20 × 20 is considered. It may be noted that to the best of authors' knowledge, the study related to skew MEE plates are not available in literature. Hence, the effectiveness of the FE formulation to assess the influence of skew angle on the plate characteristics is evaluated for the laminated composite plate by degenerating the coupling co-efficients and considering only the elastic co-efficients. The results are presented in Tables 4 and 5 for the simply supported laminated composite plate with width to thickness ratio of a/h =10 and the aspect ratio of b/a = 1. The orthotropic material properties are considered similar to Garg *et al.* (2006) and Kanasogi and Ray (2013) given as follows: $E_1/E_2 = 40$, $E_2 = E_3$, $G_{12} = 0.6E_2$, $G_{13} = G_{23} = 0.5E_2$, $\upsilon_{12} = \upsilon_{13} = \upsilon_{23} = 0.25$. The tabulated results display an excellent agreement with the results found in the literature (Garg *et al.* 2006, Kanasogi and Ray 2013). Hence, the correctness of the present FE formulation is assessed and further extended the procedure to evaluate the structural characteristics of FGSMEE plate.

4.2 Free vibration of FGSMEE plate

In this section, the free vibration characteristic of FGSMEE plate is analysed. The material property distribution is governed by the power law. Further, the FGSMEE plate having an aspect ratio of b/a = 1 and thickness ratio of a/h = 100 is evaluated for various skew angles i.e., $\alpha = 0^0$, 15^0, 30^0 and 45^0. The effect of skew angle (α) on the natural frequency corresponding to a different gradient index (i.e., η = 0, 0.2, 0.5, 1, 2, 5 and 100) is presented in Table 6 for simply supported and clamped FGSMEE plate. It can be observed that irrespective of η, the natural frequencies of the FGSMEE plate increase with the increase in skew angle. It can be attributed to the fact that the stiffness of the skew plate increase with the decrease in the plate area and the perpendicular distance between non-skew edges causing frequency enrichment. It can also be noticed that the increase in gradient index (η) values effectively decrease the natural frequencies of the FGSMEE plate. The increase in gradient index values increases the $BaTiO_3$ concentration against $CoFe_2O_4$ concentration in the FGSMEE plate. The natural frequency decreases with the increase in gradient index values is due to the lower piezoelectric elastic properties than the magnetostrictive properties. It is evident from Table 6 that the clamped FGSMEE plate yields higher natural frequency over the simply supported plate. This trend is perhaps due to the increase in local flexural rigidity of the FGSMEE plate as the edge support stiffens.

The effect of thickness ratio (a/h) on the natural frequencies of simply supported FGSMEE plate is encapsulated in Table 7 for different material gradient index and its influence on free vibration characteristics is clearly evident. The aspect ratio is considered b/a = 1 to assess the influence of different thickness ratio. The skew angle largely affects thin plates over thick and moderately thick plates. The thin plates display higher natural frequency with the increase in skew angle over thick and moderately thick plates.

Table 3 Convergence and validation studies of normalized natural frequencies of FG-MEE plate

h/a		Modes								
		1	2	3	4	5	6	7	8	9
0.2	Present (4×4)	6.798	7.923	11.283	13.595	13.642	15.202	18.982	18.693	19.326
	Present (8×8)	6.638	7.894	11.213	13.487	13.608	15.183	18.888	18.601	19.295
	Present (12×12)	6.623	7.872	11.208	13.462	13.592	15.172	18.854	18.592	19.283
	Present (16×16)	6.619	7.863	11.203	13.458	13.588	15.167	18.849	18.583	19.278
	Present (20×20)	6.618	7.860	11.198	13.455	13.583	15.161	18.843	18.579	19.273
	Milazzo (2014a)	6.735	8.223	11.882	13.463	15.049	16.951	19.027	20.178	20.415
0.1	Present (4×4)	9.720	13.598	14.909	23.158	27.195	27.290	28.106	31.411	35.006
	Present (8×8)	9.663	13.421	14.821	22.986	26.943	27.102	27.994	31.387	34.885
	Present (12×12)	9.652	13.417	14.811	22.963	26.932	27.082	27.979	31.372	34.869
	Present (16×16)	9.639	13.413	14.807	22.959	26.928	27.078	27.971	31.367	34.862
	Present (20×20)	9.637	13.408	14.801	22.952	26.921	27.069	27.967	31.361	34.858
	Milazzo (2014a)	9.584	12.852	14.733	22.577	25.701	28.339	28.734	32.391	36.341

Table 4 Non-dimensional frequency parameter $\lambda = \omega b^2/\pi^2 h(\rho/E_2)^{1/2}$ for the clamped-clamped laminated composite plate (a/h = 10)

Skew angle (α)	Source	Antisymmetric cross-ply $(0^0/90^0/0^0/90^0)$ Modes			Antisymmetric angle-ply $(45^0/-45^0/45^0/-45^0)$ Modes			Symmetric cross-ply $(90^0/0^0/90^0/0^0/90^0)$ Modes		
		1	2	3	1	2	3	1	2	3
0^0	Ref. 1	2.2990	3.7880	3.7880	2.2119	3.7339	3.7339	2.3687	3.5399	4.1122
	Ref. 2	2.3315	3.6531	3.6545	2.2433	3.6000	3.6012	2.3201	3.4769	4.4102
	Present	2.2990	3.5913	3.8695	2.1767	3.5746	3.5139	2.3400	3.3655	4.2382
15^0	Ref. 1	2.3809	3.7516	4.0785	2.3099	3.6997	4.0438	2.4663	3.6255	4.3418
	Ref. 2	2.3741	3.5856	3.8401	2.3049	3.5346	3.8092	2.3699	3.4821	4.4049
	Present	2.3992	3.5560	4.0841	2.2344	3.5111	3.9290	2.3160	3.4637	4.2346
30^0	Ref. 1	2.6666	3.9851	4.7227	2.6325	3.9549	5.2107	2.7921	3.9557	5.0220
	Ref. 2	2.5240	4.1943	4.5373	2.4945	3.6113	5.0932	2.5366	3.5696	4.4734
	Present	2.4903	3.8967	4.4609	2.4722	3.5807	5.0199	2.4896	3.6363	4.7949
45^0	Ref. 1	3.3015	4.6290	5.8423	3.3015	4.6290	5.8423	3.4739	4.7129	5.8789
	Ref. 2	2.8377	4.7614	5.6620	2.8377	4.7614	5.5162	2.8665	4.7074	5.4562
	Present	2.7948	4.5102	5.6270	2.8348	4.5102	5.4970	2.9439	4.6545	5.4362

Ref. 1: Kanasogi and Ray 2013; Ref. 2: Garg *et al*. 2006:

Table 8 presents the effect of aspect ratio on the natural frequency of the simply supported FGSMEE plate. The influence of aspect ratio is studied for a constant plate thickness ratio of a/h = 100. It can be observed from the presented results that the increase in aspect ratio leads the decrease in natural frequency of FGSMEE plate irrespective of the gradient index and skew angle. Since a and h are constants in non-dimensional frequency parameter, the increase in b will certainly decrease the frequency.

4.3 Static analysis of FGSMEE plates

This section addresses the static response characteristics of the FGSMEE plate for various geometrical conditions and material gradient index. Eq. (36) represents the sinusoidal distributed load with an applied force F_0 on the top surface of the FGSMEE plate to study the static behaviour (Lage *et al.* 2004). The geometrical parameters are considered as follows: simply supported boundary condition; a/h = 100; b/a = 1, unless otherwise stated. The effect of skew angle on the primary and secondary

Table 5 Non-dimensional frequency parameter $\lambda = \omega b^2 / \pi^2 h (\rho/E_2)^{1/2}$ for the simply supported laminated composite plate (a/h = 10)

Skew angle (α)	Source	Antisymmetric cross-ply ($0^0/90^0/0^0/90^0$) Modes			Antisymmetric angle-ply ($45^0/-45^0/45^0/-45^0$) Modes			Symmetric cross-ply ($90^0/0^0/90^0/0^0/90^0$) Modes		
		1	2	3	1	2	3	1	2	3
0^0	Ref. 1	1.4829	2.4656	3.2522	1.7974	3.3351	3.3351	1.5699	2.8917	3.7325
	Ref. 2	1.5076	2.4380	3.2254	1.8493	3.3359	3.3370	1.5635	2.4383	3.5033
	Present	1.4836	2.4392	3.1328	1.8111	3.2351	3.4889	1.5314	2.4392	3.6614
15^0	Ref. 1	1.5741	2.5351	3.0270	1.8313	3.2490	3.6724	1.6874	3.0458	3.9600
	Ref. 2	1.5796	2.5775	2.9892	1.8675	3.2075	3.5810	1.6571	2.9840	3.6505
	Present	1.5653	2.5961	3.0730	1.8219	3.1232	3.4560	1.6261	2.8245	3.5161
30^0	Ref. 1	1.8871	2.9372	3.4489	2.0270	3.4431	4.2361	2.0840	3.4023	4.6997
	Ref. 2	1.8226	2.9585	3.2357	1.9894	3.2365	4.3208	1.9596	3.1690	4.6796
	Present	1.8354	3.0573	3.4428	1.9409	3.2648	4.1836	1.9262	3.1844	4.4912
45^0	Ref. 1	2.5609	3.3126	4.0617	2.5609	3.3131	4.2772	2.8925	4.1906	5.4149
	Ref. 2	2.2996	3.4773	4.4889	2.3194	3.4870	4.5009	2.4811	4.4875	5.3289
	Present	2.3263	3.4126	4.3756	2.2676	3.4056	4.3425	2.4260	4.1908	5.2113

Ref. 1: Kanasogi and Ray 2013; Ref. 2: Garg *et al*. 2006

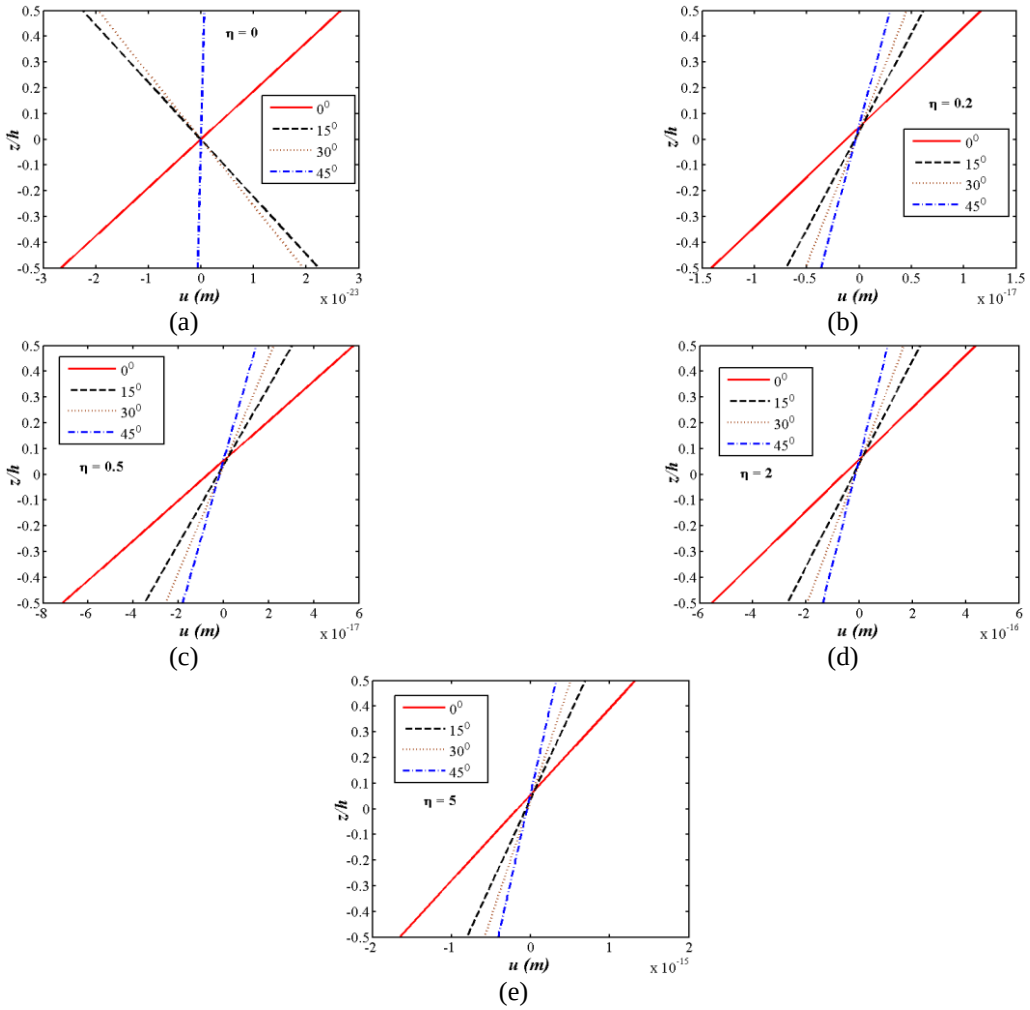

Fig. 3 Through thickness variation of displacement u for different skew angles at gradient index values (a) η = 0, (b) η = 0.2, (c) η = 0.5, (d) η = 2 and (e) η = 5

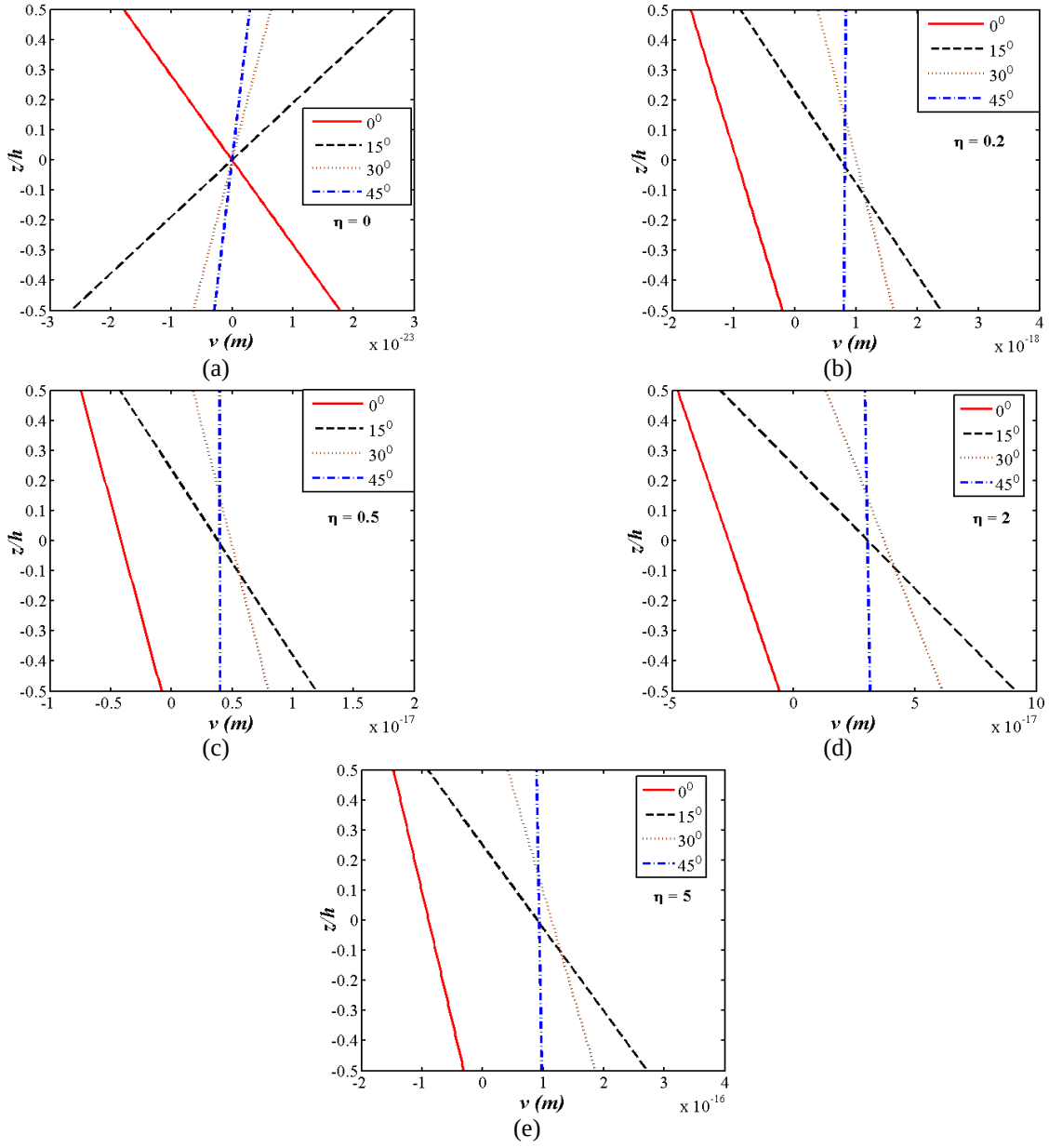

Fig. 4 Through thickness variation of displacement v for different skew angles at gradient index values (a) $\eta = 0$, (b) $\eta = 0.2$, (c) $\eta = 0.5$, (d) $\eta = 2$ and (e) $\eta = 5$

parameters is thoroughly investigated. The secondary parameters such as stresses, electric displacement, and magnetic induction are derived from the primary parameters such as displacement and potentials (electric and magnetic). Further, the effects of gradient index, boundary condition, thickness ratio and aspect ratio on the static behavior of FGSMEE plate are evaluated.

$$F_t = F_0 \sin\left(\frac{\pi x}{a}\right)\sin\left(\frac{\pi y}{b}\right) \tag{36}$$

The effect of skew angle on the displacement u across the thickness is shown in Figs. 3(a)-3(e) for the various gradient indexes. It is evident from the figures that for all the power law index values, u decreases with increase in skew angle. This is due to the fact that the stiffness of the FGSMEE plate increases with increase in skew angle. It can also be observed from these figures that for the gradient index $\eta = 0$ (i.e., pure magnetostrictive), the displacement is lower and steadily increases with the increase in gradient-index value. This may be attributed to the fact that with the increase in power law indeed (η), the volume fraction of $BaTiO_3$ increases. Since the elastic properties of $BaTiO_3$ are lower than $CoFe_2O_4$, the displacements produced are higher for higher value of η. Fig. 3 depicts the effect of skew angle on the displacement for varios gradient index values. It may be seen from Fig. 3 that for all the skew angles, the displacement quantity u across the thickness direction

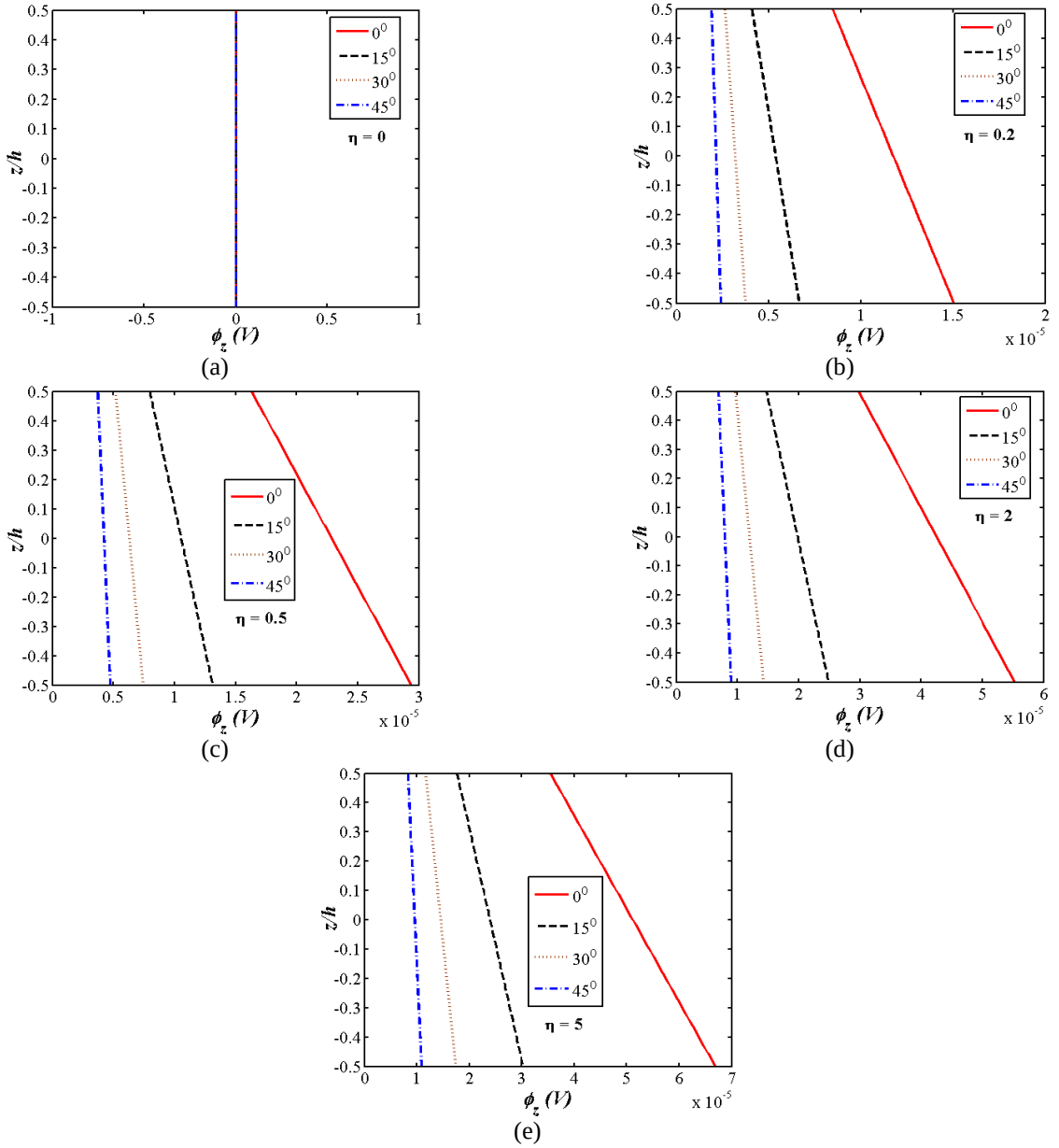

Fig. 5 Through thickness variation of electric potential ϕ_z for different skew angles at gradient index values (a) η = 0, (b) η = 0.2, (c) η = 0.5, (d) η = 2 and (e) η = 5

experiences only bending. Figs. 4(a)-4(e) present the through-thickness behavior of the displacement quantity *v* across the z-direction. It can be observed from the Fig. 4(a) that for η = 0, the FGSMEE plate experiences only bending for all the skew angles while stretching is dominant for other gradient index values. The increase in gradient-index values witnessed an increase in stretching and decrease in bending of the plate. This phenomenon can be attributed to the piezoelectric material possesing a tendency to increase the stiffness of the plate in the polling direction by induced electric field due to the strains developed (Ray *et al.* 1992, Bhangale and Ganesan 2006). Hence, the plate with low $BaTiO_3$ concentration experiences lower induced electric field resulting in bending only. The increase in $BaTiO_3$ concentration causes the increase in induced electric field in the polling direction i.e., *z*-direction, there by reduces the bending in the thickness direction and increases stretching along in-plane direction.

The effect of skew angle on electric and magnetic potentials is investigated. The slope in *the* z-direction for electric potential decreases with the increase in skew angle as observed from Figs. 5(a)-5(e). It can also be seen that the electric potential ϕ increase with the increase in η. This is due to piezoelectric enrichment of FGSMEE plate due to increase in the η. Similarly, the effect of skew angle on the magnetic potential of FGSMEE plate for various gradient index η is shown in Figs. 6(a)-6(e). It is noticed from these figures that the magnetic potential vary linearly symmetric across the thickness (negative potential at the bottom and positive at the top). It can also be noticed that the magnetic

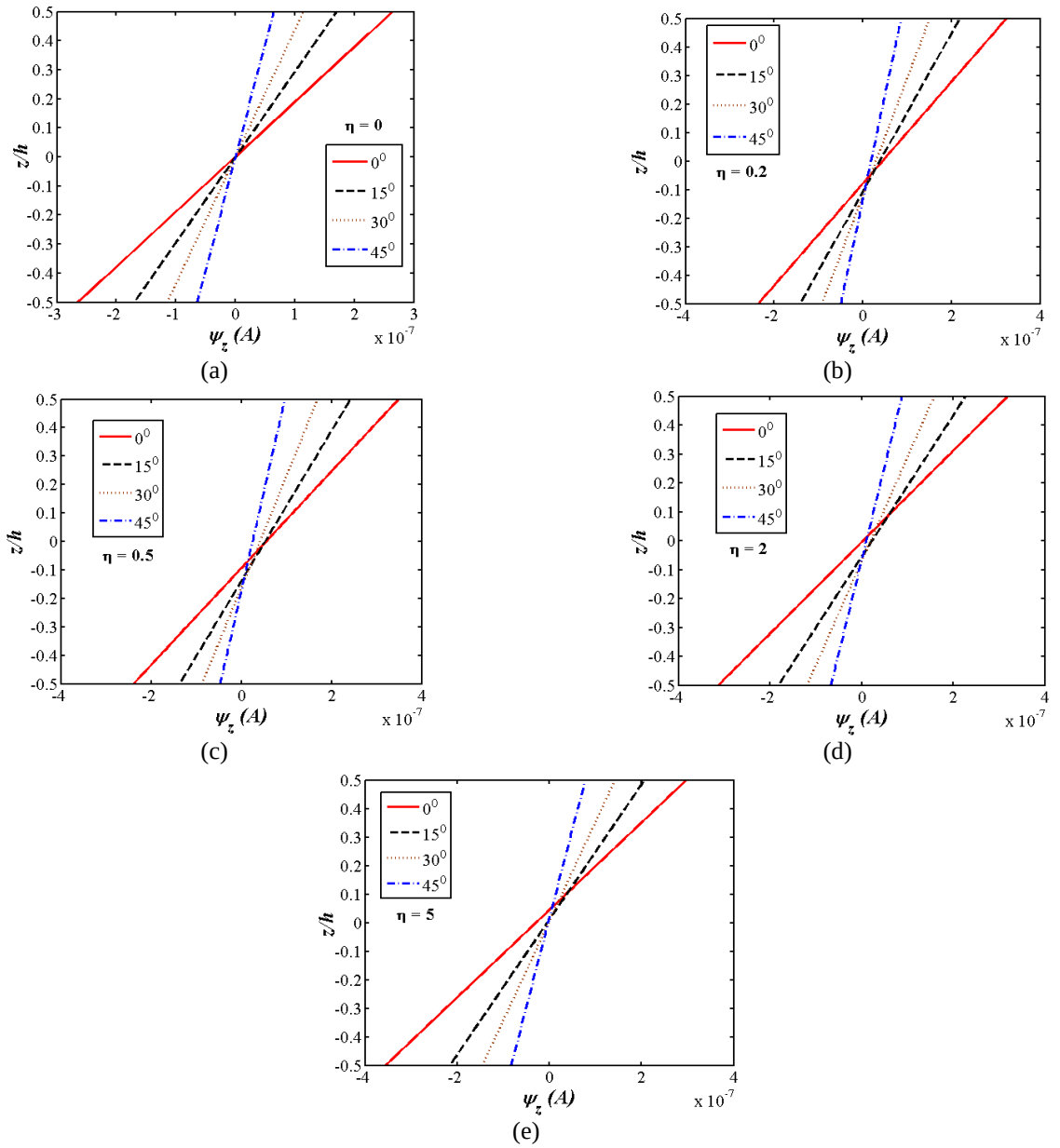

Fig. 6 Through thickness variation of magnetic potential ψ_z for different skew angles at gradient index values (a) $\eta = 0$, (b) $\eta = 0.2$, (c) $\eta = 0.5$, (d) $\eta = 2$ and (e) $\eta = 5$

potential decreases with the increase in skew angle, irrespective of gradient index. Further, the increase in gradient-index values had minimal effect on magnetic potential.

The effect of skew angle (α) on the normal stress (σ_{xx}) for different gradient index is given in Figs. 7(a)-7(e). The normal stress (σ_{xx}) for FGSMEE plate with zero skew angle ($\alpha = 0^0$) and gradient index $\eta = 0$, linearly vary across the thickness. The bottom half of the plate experiences compressive stress while the top half experiences tensile stress as shown in Fig. 7(a). For $\eta > 0$, the through-thickness variation of σ_{xx} appears to be non-linear whereas, at $\eta = 0$, the behavior is linear. For FGSMEE plate with the skew angle $\alpha = 15^0$, 30^0, and 45^0, irrespective of gradient index η, the lower half of the plate experience tensile stress while the upper half experience compressive stress. Further, for FGSMEE plate with $\eta = 0$, the normal stress (σ_{xx}) increases for $\alpha = 15^0$, 30^0 while for $\alpha = 45^0$, a decrease in the normal stress (σ_{xx}) is seen. Similar trends can be observed for other gradient index values. The normal stress (σ_{yy}) can be seen in Figs. 8(a)-8(e) having the similar behavior of σ_{xx} for all the considered cases. The effect of skew angle on the in-plane shear stress (τ_{xy}) of FGSMEE plate is reported in Figs. 9(a)-9(e) corresponding to various η values. The in-plane shear stress (τ_{xy}) increases with the increase in skew angle for all the considered gradient index values.

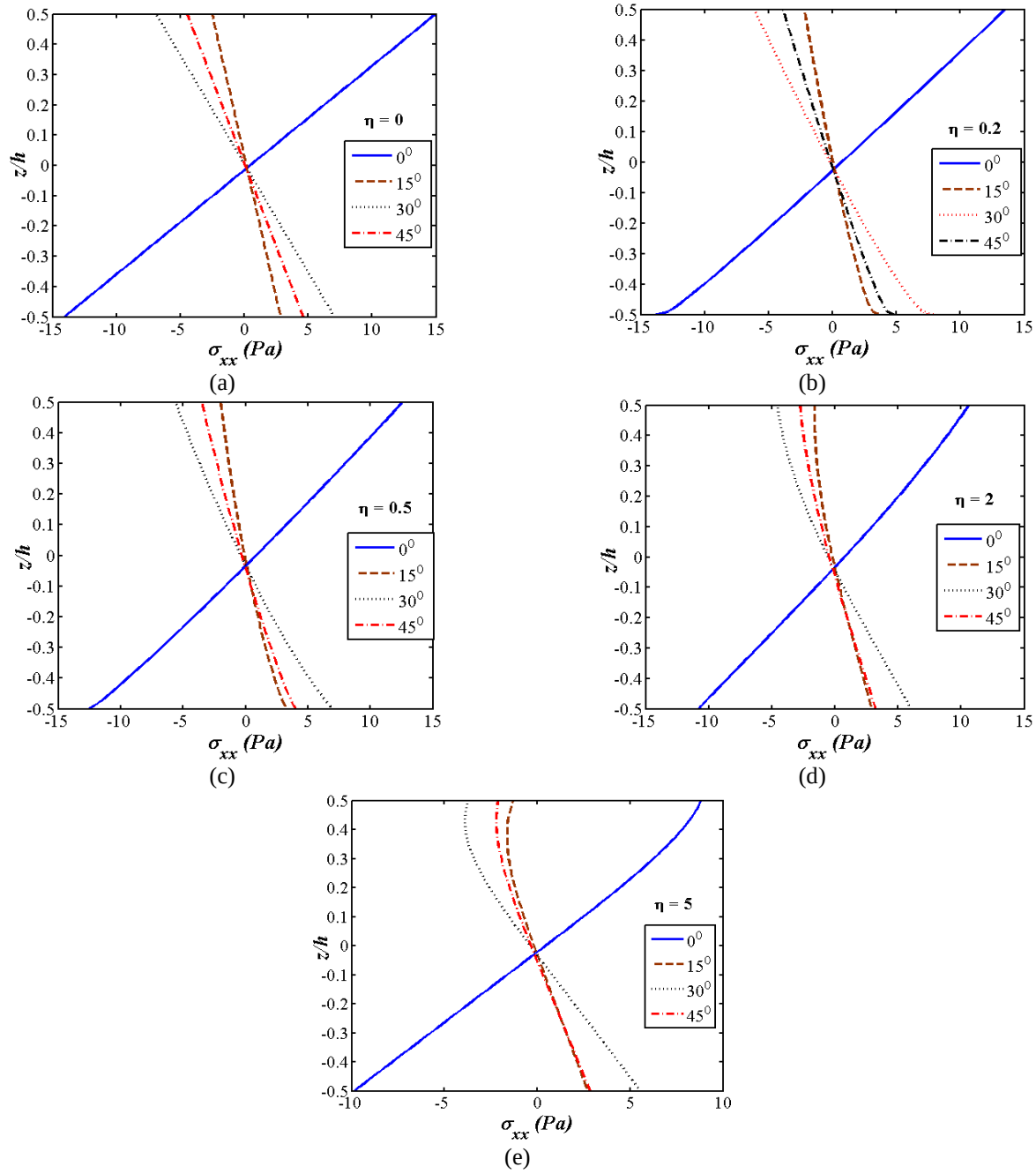

Fig. 7 Through thickness variation of normal stress σ_{xx} for different skew angles at gradient index values (a) $\eta = 0$, (b) $\eta = 0.2$, (c) $\eta = 0.5$, (d) $\eta = 2$ and (e) $\eta = 5$

Figs. 10(a)-10(e) present the transverse shear stress (τ_{xz}) distribution across the thickness of various gradient index values. It can be clearly seen from the Fig. 10 that the transverse shear stress decreases with the increase in skew angle.

Through the thickness variation of magnetic induction (B_z) and electric displacement (D_z) for different skew angles and gradient index values is presented in Figs. 11(a)-11(e) and 12(a)-12(e), respectively. For the case of a pure magnetostrictive plate, as seen in Fig 11(a), the magnetic induction decreases with the increase in skew angle for $\alpha \leq 30^0$. It can also be observed that for skew angle $\alpha \leq 30^0$, the plate experiences linear variation with positive B_z at the bottom surface of the plate and negative at the top surface. However, for $\alpha = 45^0$, the FGSMEE plate exhibit negative B_z at the bottom half of the plate and positive at the top half of the plate. For certain gradient index values (i.e., $\eta = 0.2$, 0.5, 2 and 5), the bottom surface of the FGSMEE plate experiences nearly zero magnetic induction B_z irrespective of the skew angle.

Table 6 Influence of skew angle on the natural frequency of FGSMEE plate

Skew angle (α)	Power law index η	Boundary condition	Natural frequencies				
			1	2	3	4	5
0^0	0	SSSS	4.561	11.782	11.848	23.655	25.466
		CCCC	10.646	22.006	22.066	33.028	36.367
	0.2	SSSS	4.357	11.292	11.327	22.850	24.462
		CCCC	10.357	21.322	21.363	31.924	35.230
	0.5	SSSS	4.240	11.010	11.029	22.376	23.882
		CCCC	10.116	20.755	20.781	31.021	34.297
	2	SSSS	4.123	10.726	10.731	21.884	23.296
		CCCC	9.748	19.894	19.900	29.673	32.891
	5	SSSS	4.053	10.555	10.558	21.604	22.941
		CCCC	9.588	19.520	19.522	29.094	32.278
	100	SSSS	3.927	10.240	10.255	21.110	22.293
		CCCC	9.190	18.549	18.574	27.616	30.705
15^0	0	SSSS	6.600	12.600	14.638	24.289	28.824
		CCCC	11.231	22.753	23.996	35.284	39.202
	0.2	SSSS	6.346	12.081	14.038	23.396	27.660
		CCCC	10.923	22.065	23.236	34.111	37.980
	0.5	SSSS	6.197	11.783	13.692	22.876	26.990
		CCCC	10.668	21.493	22.607	33.149	36.980
	2	SSSS	6.045	11.483	13.342	22.342	26.312
		CCCC	10.277	20.621	21.656	31.711	35.477
	5	SSSS	5.957	11.306	13.137	22.034	25.917
		CCCC	10.107	20.243	21.247	31.092	34.824
	100	SSSS	5.799	10.989	12.769	21.490	25.215
		CCCC	9.685	19.283	20.201	29.514	33.147
30^0	0	SSSS	8.805	16.015	20.886	29.138	37.879
		CCCC	13.385	26.297	29.852	43.037	48.861
	0.2	SSSS	8.424	15.376	19.994	27.979	36.326
		CCCC	13.008	25.552	28.913	41.657	47.347
	0.5	SSSS	8.203	15.009	19.480	27.308	35.424
		CCCC	12.696	24.932	28.138	40.518	46.106
	2	SSSS	7.981	14.636	18.964	26.627	34.511
		CCCC	12.220	23.984	26.967	38.801	44.242
	5	SSSS	7.851	14.417	18.659	26.231	33.979
		CCCC	12.014	23.571	26.463	38.060	43.435
	100	SSSS	7.618	14.028	18.112	25.530	33.025
		CCCC	11.500	22.532	25.177	36.168	41.370
45^0	0	SSSS	13.156	22.879	34.065	41.884	57.023
		CCCC	18.884	34.854	44.131	59.703	71.843
	0.2	SSSS	12.553	21.988	32.526	40.222	54.670
		CCCC	18.336	33.891	42.749	57.994	69.709
	0.5	SSSS	12.205	21.474	31.642	39.255	53.297
		CCCC	17.883	33.095	41.608	56.571	67.954
	2	SSSS	11.858	20.951	30.759	38.271	51.908
		CCCC	17.195	31.880	39.886	54.393	65.303
	5	SSSS	11.654	20.647	30.238	37.700	51.099
		CCCC	16.896	31.352	39.145	53.444	64.152
	100	SSSS	11.287	20.110	29.298	36.682	49.642
		CCCC	16.149	30.042	37.253	51.045	61.219

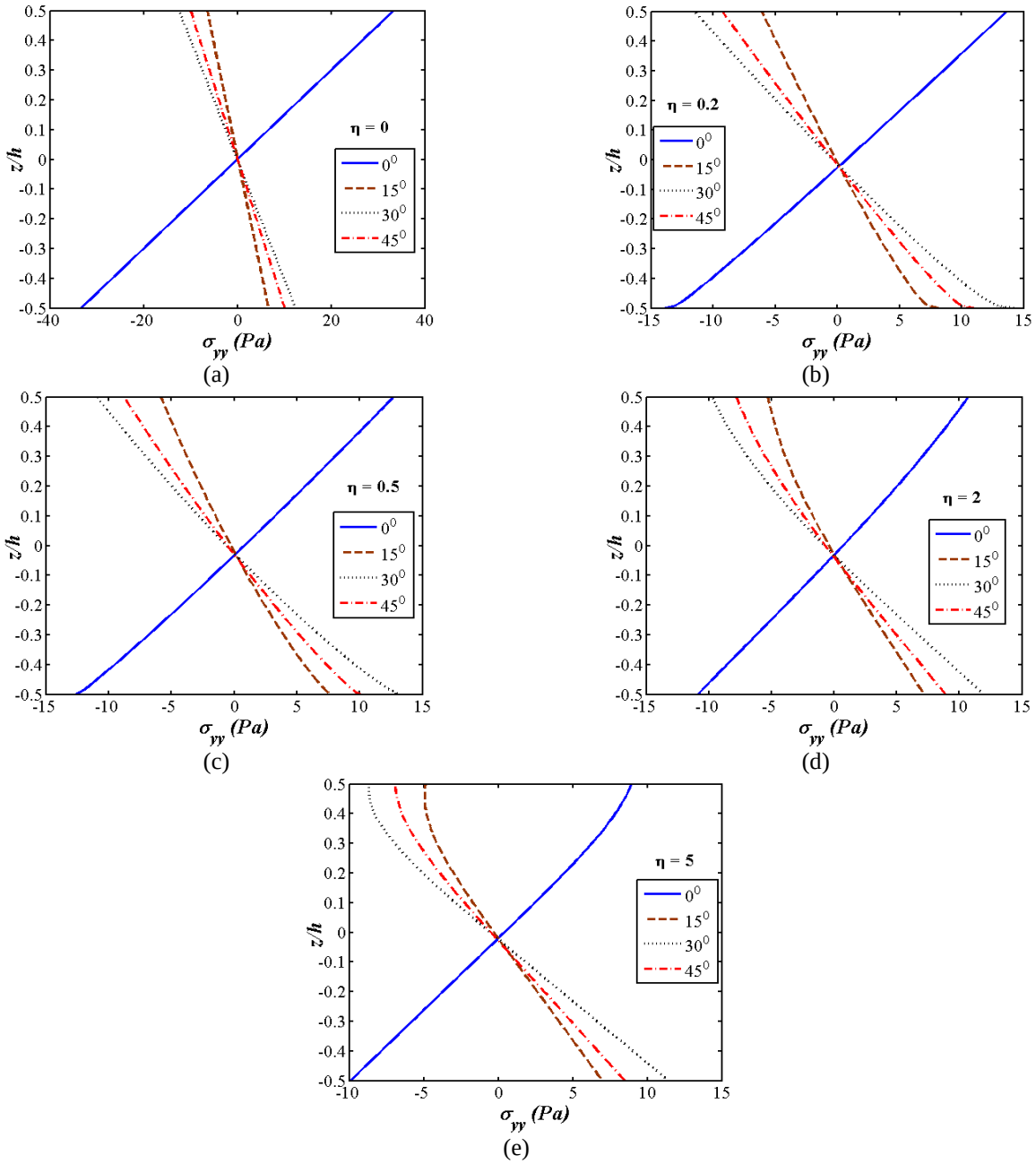

Fig. 8 Through thickness variation of normal stress σ_{yy} for different skew angles at gradient index values (a) $\eta = 0$, (b) $\eta = 0.2$, (c) $\eta = 0.5$, (d) $\eta = 2$ and (e) $\eta = 5$

Further, it is seen from Figs. 11(b)-11(e) that the magnitude of B_z decreases with the increase in skew angle. For the case of a pure magnetostrictive plate as seen in Fig. 12(a), no influence of skew angle on the electric displacement D_z is observed. For rest of the gradient index values (i.e., $\eta = 0.2$, 0.5, 2 and 5), the top surface of the FGSMEE plate experience zero electric displacement D_z, irrespective of skew angle (α). The magnitude of D_z decreases with the increase in α. The square ($\alpha = 0^0$) FGSMEE plate experiences positive D_z for all the η values while the increase in α leads to negative D_z for all η values.

The effect of aspect ratio on the static behavior of FGSMEE plate is presented in Figs. 13(a)-13(j). The plotted results are obtained for the thickness ratio of $a/h = 100$. From the plots, it can be seen that aspect ratio has a significant influence on the primary and secondary quantities. The displacements u and v increases for the aspect ratio $b/a = 2$ in comparison with $b/a = 1$. The potentials display an increase in the magnitude and amongst them, the influence on electric potential is found to be more dominant.

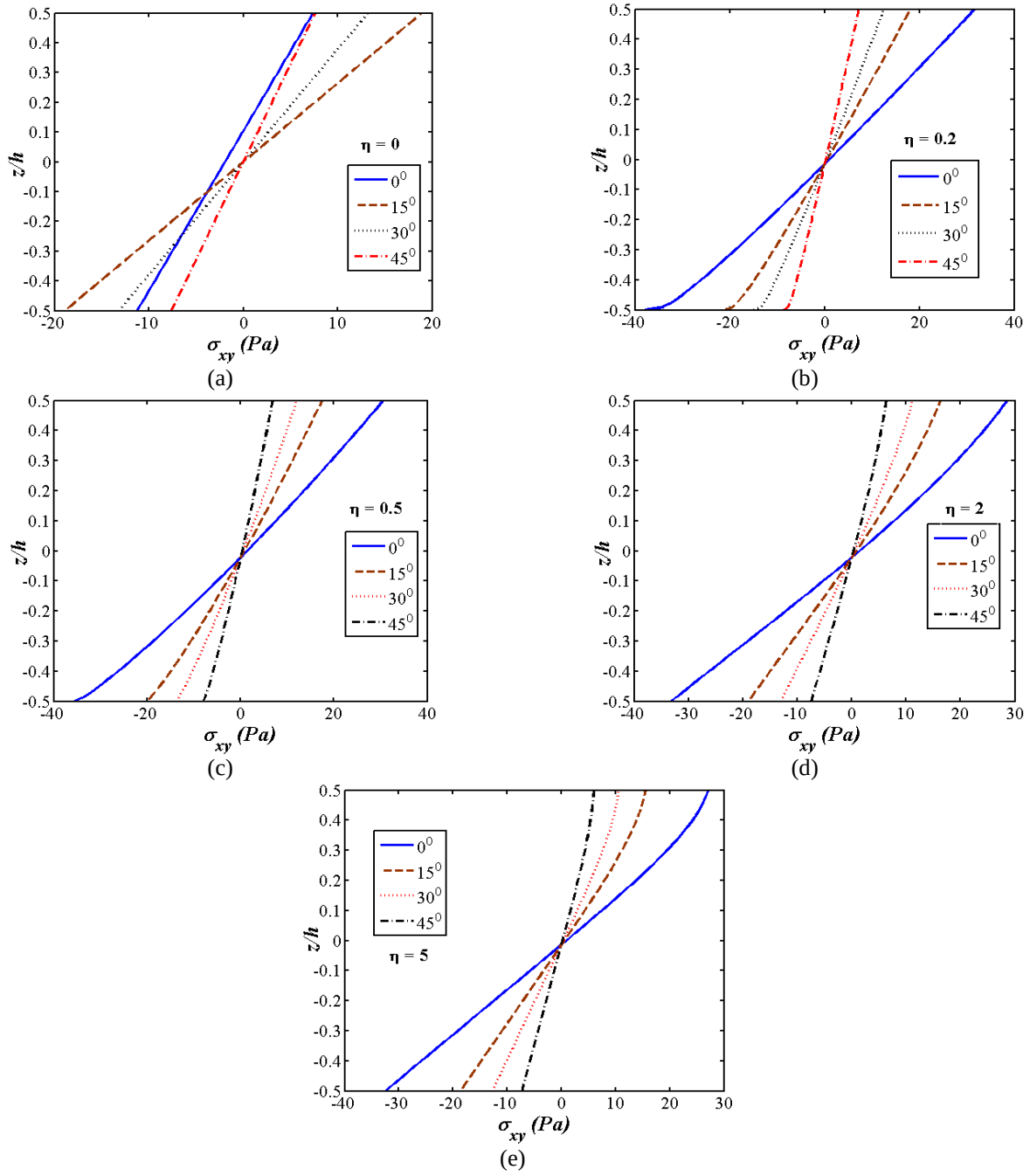

Fig. 9 Through thickness variation of normal stress σ_{xy} for different skew angles at gradient index values (a) η = 0, (b) η = 0.2, (c) η = 0.5, (d) η = 2 and (e) η = 5

The normal stress (σ_{xx}) experiences tension at the bottom half and compression at the top half for the square FGSMEE plate while for a plate with b/a = 2, the bottom half experiences compression and the top half experiences tension. The normal stress σ_{yy} and in-plane shear stress (τ_{xy}) increases with the increase in the lateral dimension of the plate. The transverse shear stress (τ_{xz}) decreases with the increase in aspect ratio. The magnetic induction (B_z) decreases for higher aspect ratio while the higher aspect ratio produces a nearly constant electric displacement (D_z) at the bottom half of the FGSMEE plate. Figs. 14(a) -14(j) present the effect of geometrical parameter thickness ratio on primary and secondary parameters of FGSMEE plate subjected to a static load. It can be seen from the plots that the a/h ratio has considerable influence on the static behavior of FGSMEE plate. The effect of thickness ratio on static behavior is assessed for the FGSMEE plate having dimension b/a = 1. The primary quantities i.e., displacements (u and v) and potentials (electric and magnetic), increases with the increase in thickness ratio.

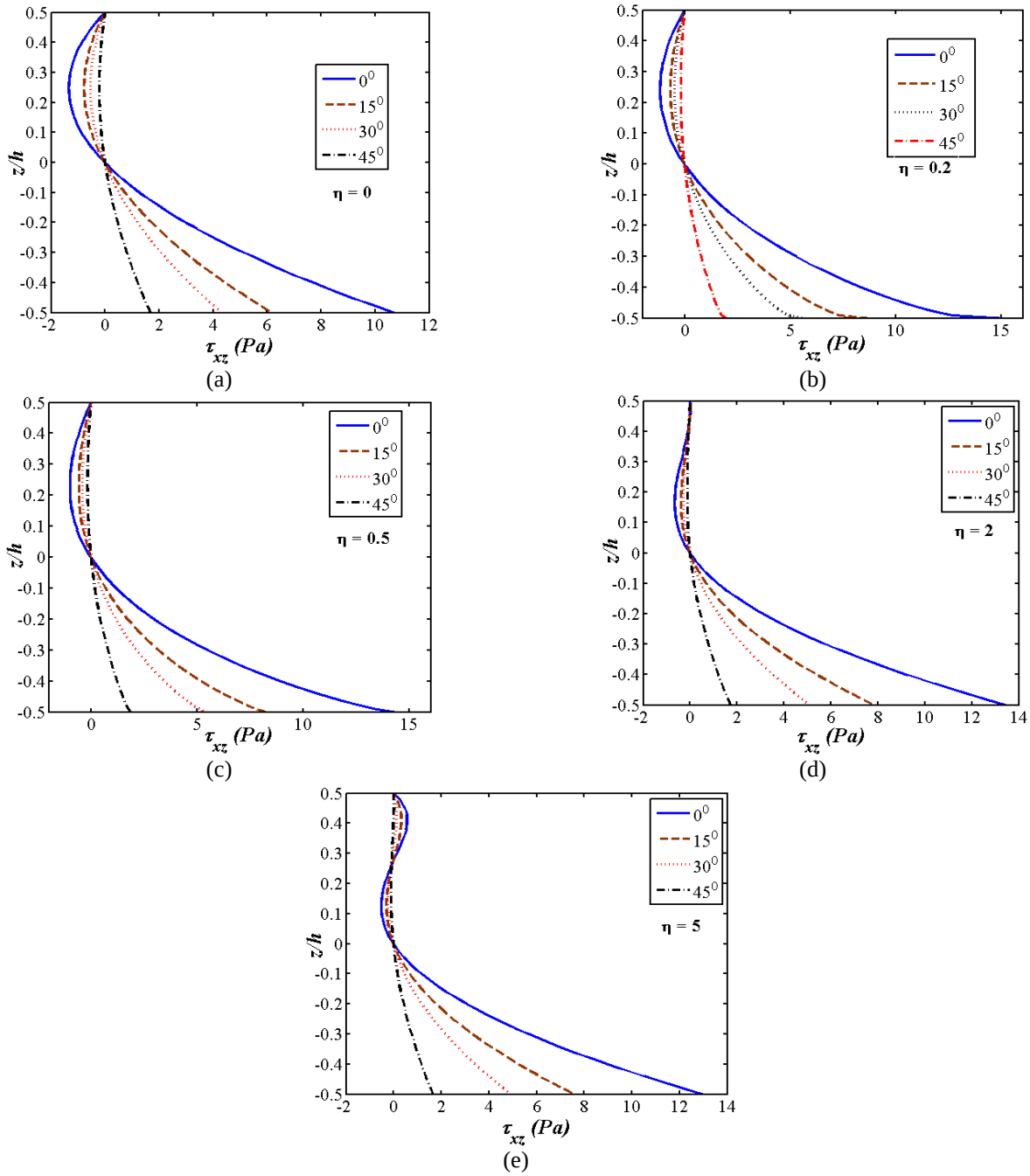

Fig. 10 Through thickness variation of shear stress τ_{xz} for different skew angles at gradient index values (a) η = 0, (b) η = 0.2, (c) η = 0.5, (d) η = 2 and (e) η = 5

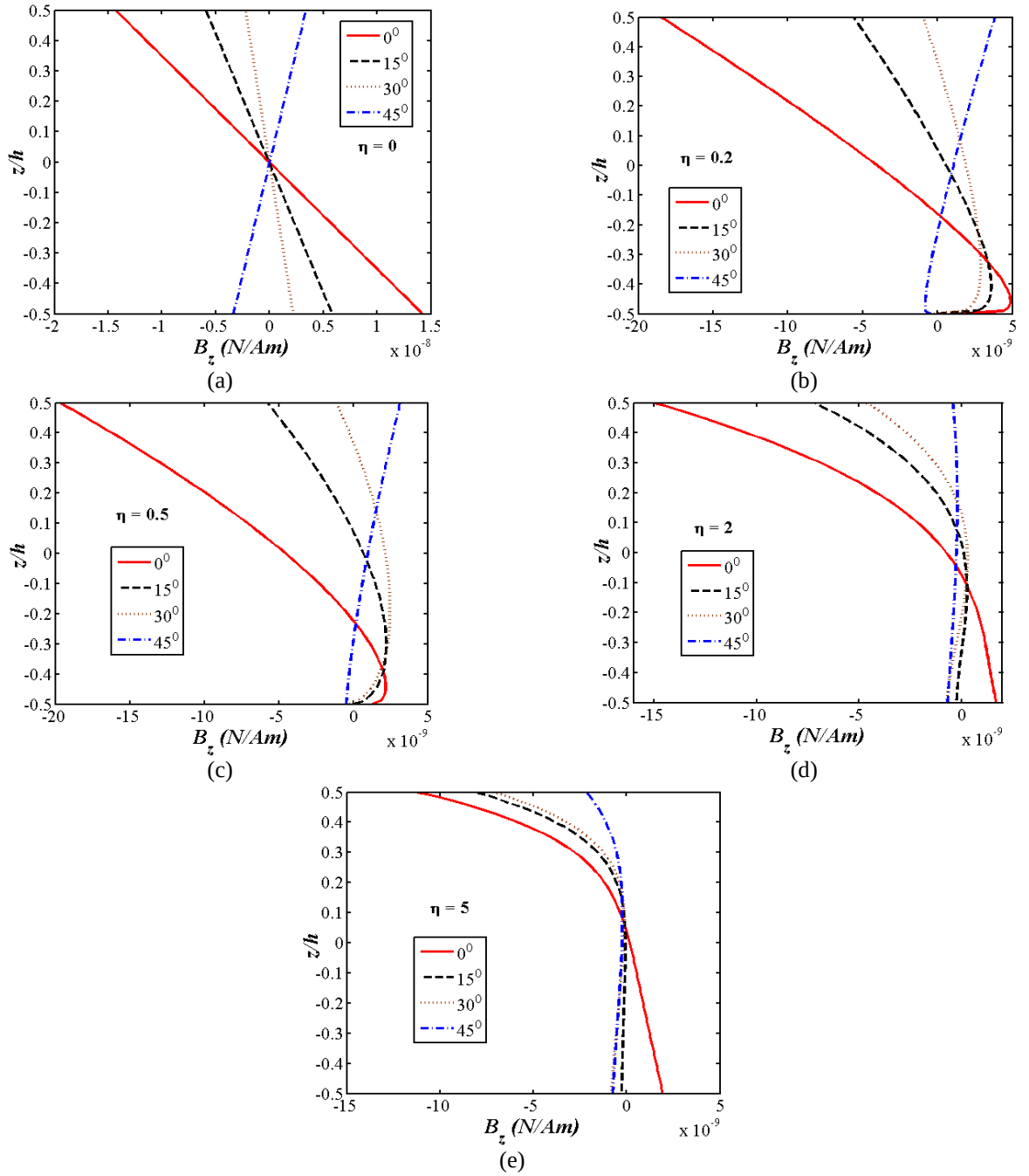

Fig. 11 Through thickness variation of magnetic induction B_z for different skew angles at gradient index values (a) $\eta = 0$, (b) $\eta = 0.2$, (c) $\eta = 0.5$, (d) $\eta = 2$ and (e) $\eta = 5$

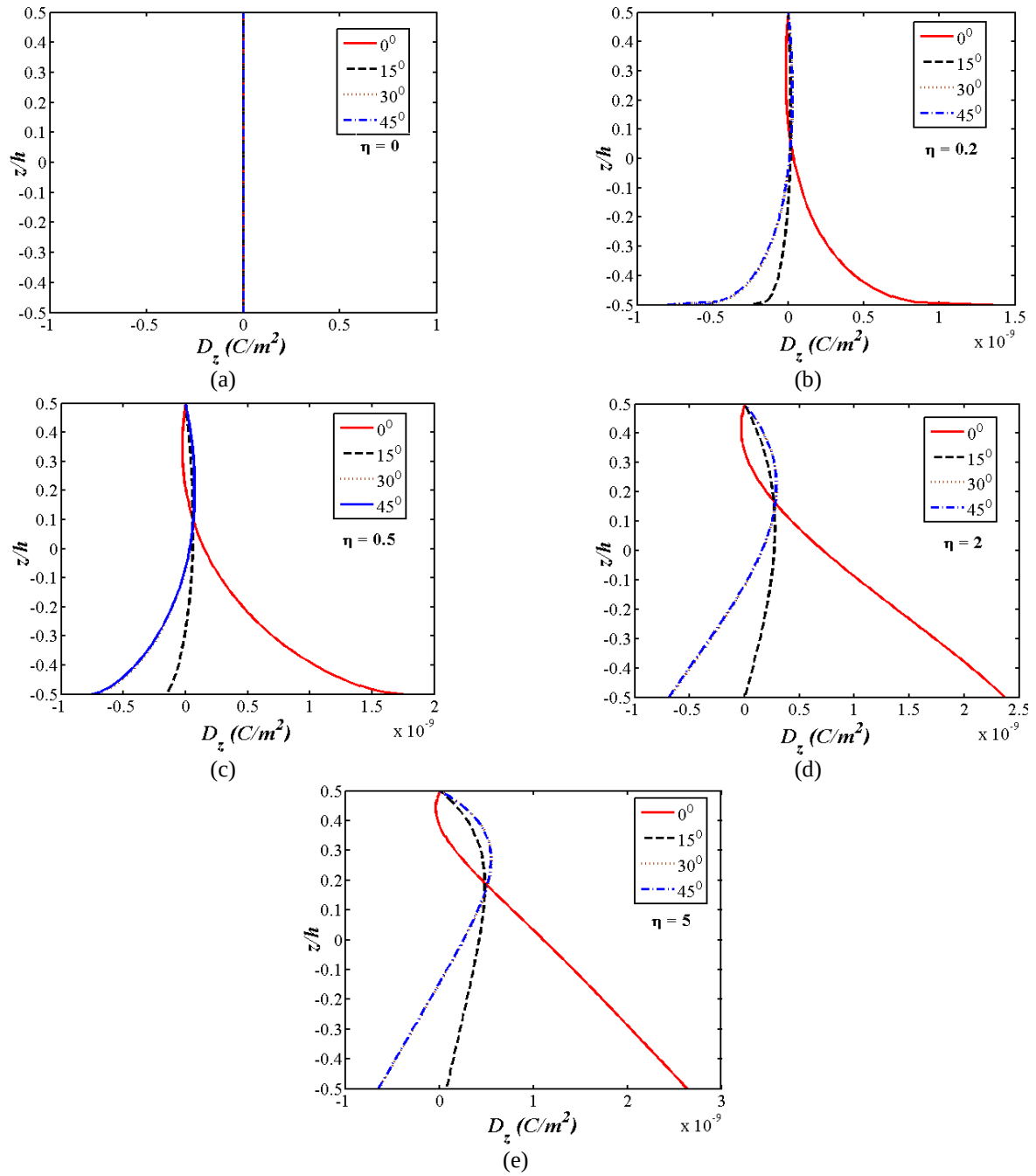

Fig. 12 Through thickness variation of electric displacement D_z for different skew angles at gradient index values (a) η = 0, (b) η = 0.2, (c) η = 0.5, (d) η = 2 and (e) η = 5

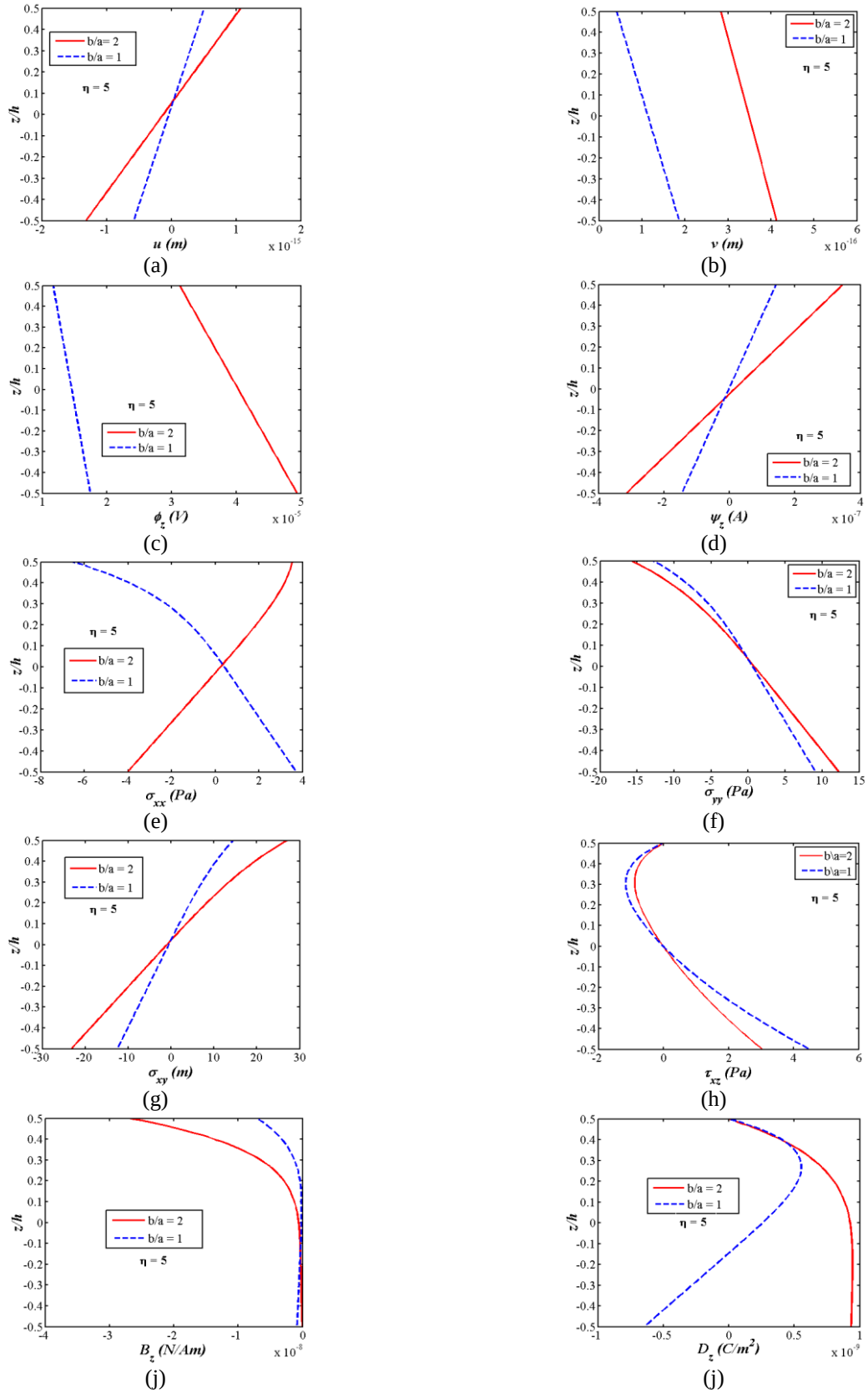

Fig. 13 Effect of aspect ratio (b/a) on (a) u, (b) v, (c) ϕ_z, (d) Ψ_z, (e) σ_{xx}, (f) σ_{yy}, (g) σ_{xy} , (h) τ_{xz} , (i) B_z and (j) D_z

Table 7 Influence of thickness ratio (a/h) on the natural frequency of FGSMEE plate

Skew angle (α)	a/h	η =0			η =0.2			η =1			η =2			η =5			η =100		
		1	2	3	1	2	3	1	2	3	1	2	3	1	2	3	1	2	3
	10	4.296	10.206	10.253	4.181	9.963	9.996	4.007	9.589	9.601	3.944	9.4539	9.4591	3.881	9.315	9.316	3.721	8.952	8.971
0^0	20	4.477	11.316	11.376	4.350	11.008	11.049	4.120	10.251	10.265	4.053	10.092	10.098	3.986	9.930	9.932	3.813	9.499	9.521
	100	4.561	11.782	11.848	4.357	11.292	11.327	4.173	10.846	10.858	4.123	10.726	10.731	4.053	10.555	10.558	3.927	10.240	10.255
	10	4.671	10.149	11.643	4.550	9.903	11.370	4.367	9.526	10.950	4.302	9.389	10.797	4.236	9.251	10.642	4.068	8.905	10.257
15^0	20	4.985	11.075	12.837	4.853	10.777	12.498	4.655	10.326	11.985	4.584	10.166	11.802	4.512	10.003	11.617	4.331	9.590	11.146
	100	6.600	12.600	14.638	6.346	12.081	14.038	6.110	11.611	13.491	6.045	11.483	13.342	5.957	11.306	13.137	5.799	10.989	12.769
	10	5.960	11.379	15.015	5.817	11.118	14.692	5.598	10.716	14.191	5.519	10.569	14.006	5.439	10.421	13.820	5.241	10.054	13.363
30^0	20	6.700	12.866	17.418	6.531	12.535	16.983	6.274	12.033	16.319	6.182	11.853	16.081	6.089	11.671	15.839	5.856	11.212	15.232
	100	8.805	16.015	20.886	8.424	15.376	19.994	8.075	14.795	19.183	7.981	14.636	18.964	7.851	14.417	18.659	7.618	14.028	18.112
	10	8.926	14.698	18.558	8.725	14.390	18.209	8.414	13.911	17.519	8.301	13.734	17.162	8.186	13.555	16.798	7.906	13.123	16.441
45^0	20	10.464	17.471	27.455	10.197	17.039	26.832	9.788	16.379	25.856	9.641	16.141	25.487	9.492	15.900	25.114	9.122	15.298	24.183
	100	13.156	22.879	34.065	12.553	21.988	32.526	12.005	21.174	31.133	11.858	20.951	30.759	11.654	20.647	30.238	11.287	20.110	29.298

Table 8 Influence of aspect ratio (b/a) on the natural frequency of FGSMEE plat

Skew angle (α)	b/a	η =0			η =0.2			η =1			η =2			η =5			η =100		
		1	2	3	1	2	3	1	2	3	1	2	3	1	2	3	1	2	3
	0.5	9.611	16.192	29.925	10.000	16.809	30.965	10.434	17.508	32.156	10.594	17.768	32.603	10.792	18.089	33.149	11.164	18.694	34.166
0^0	1	4.561	11.782	11.848	4.357	11.292	11.327	4.173	10.846	10.858	4.123	10.726	10.731	4.053	10.555	10.558	3.927	10.240	10.255
	1.5	2.790	5.946	8.842	2.906	6.153	9.201	3.036	6.389	9.609	3.084	6.478	9.761	3.144	6.586	9.948	3.257	6.788	10.305
	2	2.417	4.498	8.393	2.518	4.651	8.741	2.631	4.826	9.135	2.673	4.892	9.282	2.725	4.972	9.463	2.824	5.120	9.807
	0.5	14.830	20.501	33.669	15.287	21.166	34.759	15.811	21.933	36.018	16.008	22.222	36.494	16.246	22.575	37.074	16.675	23.226	38.144
15^0	1	6.600	12.600	14.638	6.346	12.081	14.038	6.110	11.611	13.491	6.045	11.483	13.342	5.957	11.306	13.137	5.799	10.989	12.769
	1.5	3.790	6.533	9.965	3.928	6.766	10.3654	4.085	7.032	10.818	4.144	7.132	10.986	4.217	7.253	11.194	4.349	7.482	11.586
	2	3.067	4.885	9.175	3.186	5.056	9.557	3.321	5.251	9.990	3.372	5.324	10.151	3.434	5.414	10.349	3.548	5.579	10.727
	0.5	22.054	28.411	43.822	22.872	29.397	45.211	23.795	30.525	46.819	24.140	30.949	47.427	24.560	31.467	48.167	25.329	32.422	49.526
30^0	1	8.805	16.015	20.886	8.424	15.376	19.994	8.075	14.795	19.183	7.981	14.636	18.964	7.851	14.417	18.659	7.618	14.028	18.112
	1.5	4.793	8.597	12.897	4.975	8.913	13.424	5.183	9.274	14.019	5.261	9.408	14.241	5.357	9.573	14.514	5.535	9.884	15.028
	2	3.859	6.293	11.586	4.012	6.525	12.071	4.184	6.789	12.618	4.248	6.888	12.821	4.328	7.010	13.073	4.474	7.237	13.549
	0.5	34.859	43.221	64.861	36.288	44.836	66.984	37.896	46.678	69.432	38.497	47.369	70.360	39.236	48.217	71.488	40.600	49.791	73.558
45^0	1	13.156	22.879	34.065	12.553	21.988	32.526	12.005	21.174	31.133	11.858	20.951	30.759	11.654	20.647	30.238	11.287	20.110	29.298
	1.5	6.878	13.199	19.584	7.152	13.679	20.382	7.462	14.227	21.283	7.579	14.433	21.618	7.722	14.684	22.033	7.989	15.153	22.810
	2	5.557	9.715	17.426	5.774	10.083	18.146	6.020	10.501	18.957	6.112	10.657	19.258	6.226	10.850	19.630	6.435	11.208	20.332

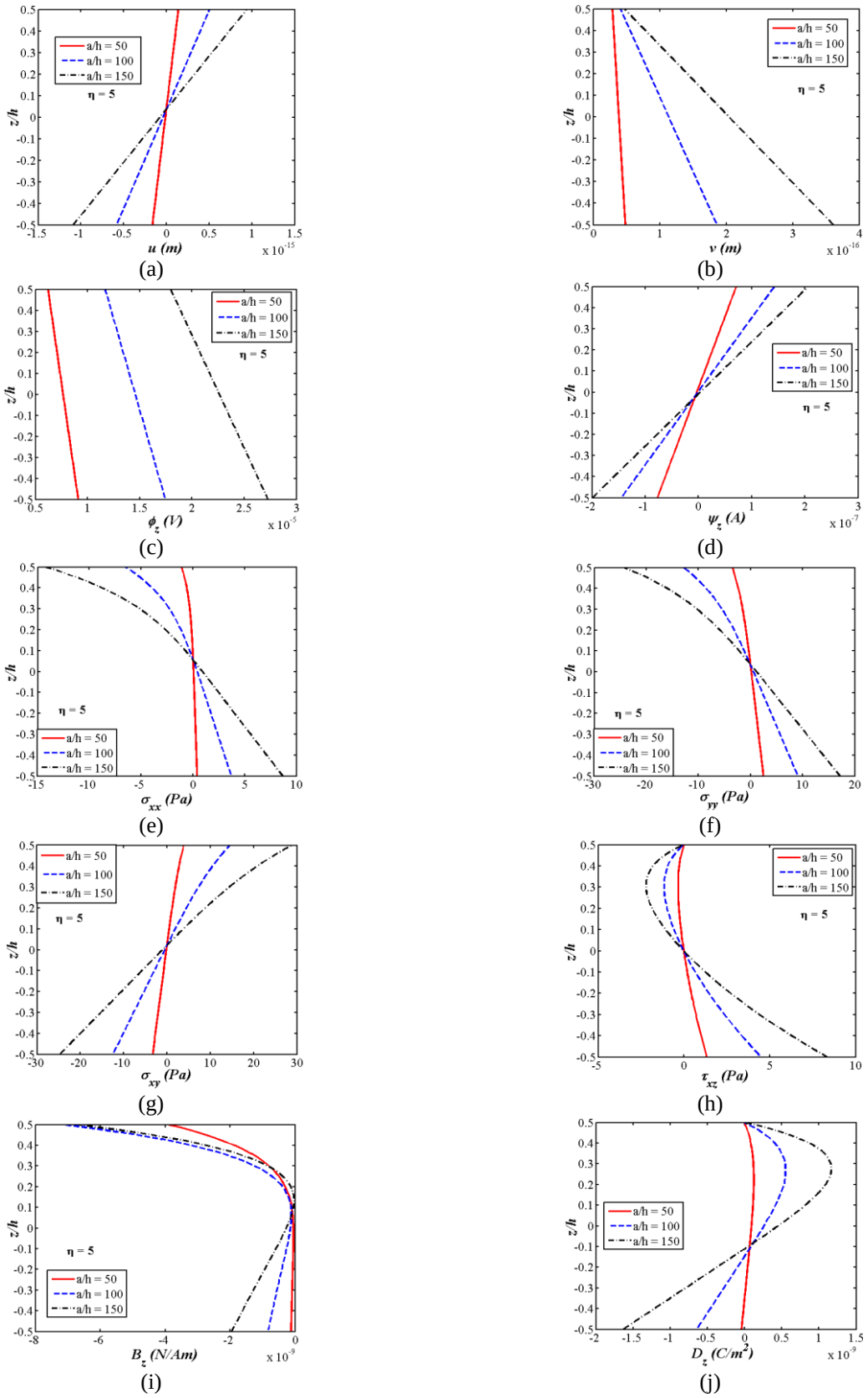

Fig. 14 Effect of thickness ratio (a/h) on (a) u, (b) v, (c) ϕ_z, (d) Ψ_z, (e) σ_{xx}, (f) σ_{yy}, (g) σ_{xy}, (h) τ_{xz}, (i) B_z and (j) D_z

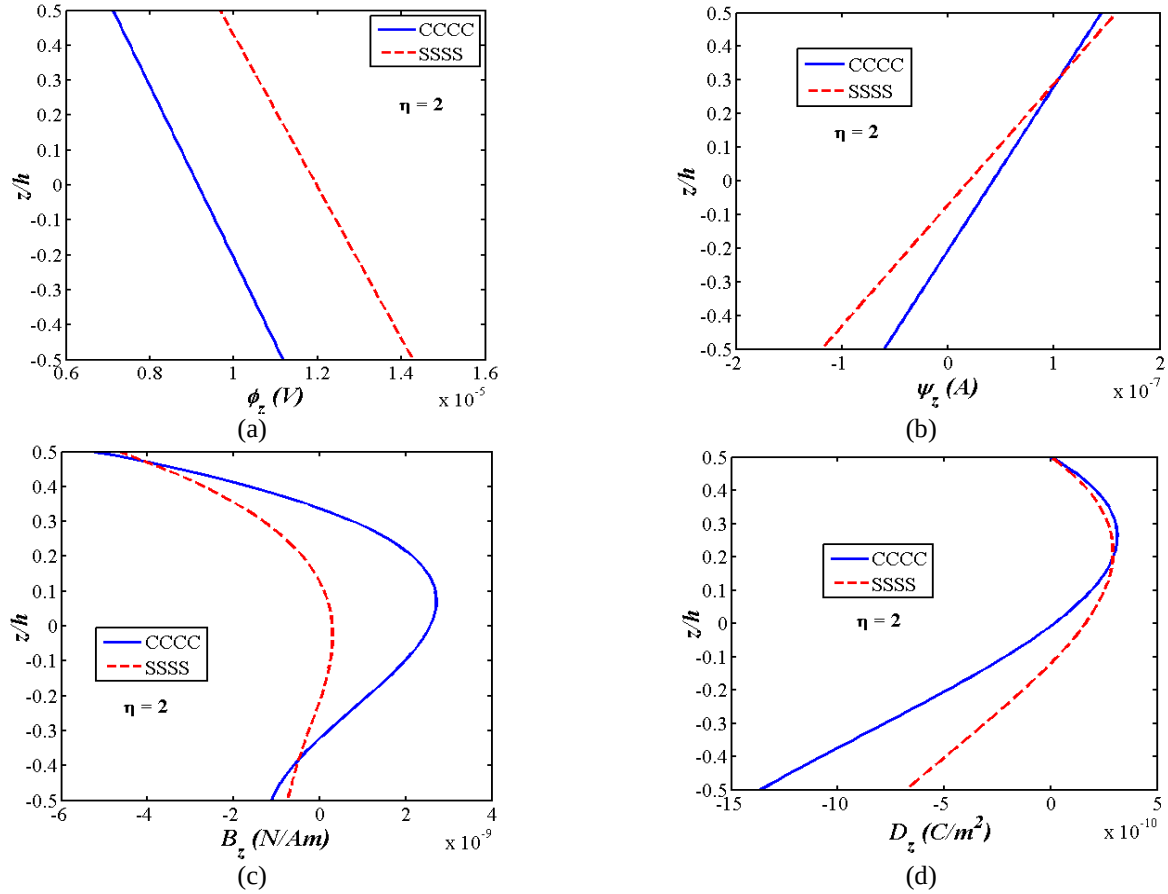

Fig. 15 Effect of boundary condition on (a) ϕ_z, (b) Ψ_z, (c) B_z and (d) D_z

The effect of boundary condition on the static response of FGSMEE plate is presented in Figs. 15(a)-15(d). These figures suggest that a considerable influence on the plotted parameters, i.e., ϕ_z, Ψ_z, B_z, and D_z is observed as the boundary restraint changes from simply supported edges to clamped edges. The trend is due to the increase in local flexural rigidity of the plate with stiffening edge support.

5. Conclusions

In this article, a finite element formulation to analyze the free vibration and static behavior of FGSMEE plate is developed and implemented. To investigate the behavior of the FGSMEE plate, the transformation matrix between the global and local degrees of freedom for the nodes lying on the skew edges has been successfully incorporated. Graded material distribution along the thickness has been achieved using a simple power law and rule of mixture. The influence of skew angle on the natural frequencies of the FGSMEE plate has been effectively investigated. Further, the static behavior of FGSMEE plate is evaluated thoroughly in terms of primary and secondary structural parameters such as the displacements, electric potential, magnetic potential, stresses, electric displacement, and magnetic induction. In addition, the influence of material gradient index is also studied. Further, the effect of boundary conditions, thickness ratio, and aspect ratio on the structural behaviour of the FGSMEE plates is thoroughly investigated. Some of the key findings of the present studies are listed below:

- The free vibration studies for FGSMEE plate unveiled that the natural frequency increases with the increase in the skew angle irrespective of the material gradient index values.
- It is observed that the natural frequency decreases with the increase in gradient-index values.
- The electric and magnetic potential decreases with the increase in the skew angle.
- The gradient index η exhibits major influence on the electric potential while its influence on the magnetic potential is observed to be minimal.
- The magnitude of electric displacement (D_z) and magnetic induction (B_z) decreases with the increase in the skew angle.
- The free vibration and static response characteristics are significantly affected by the thickness ratio, aspect ratio, and the boundary conditions.

References

Adineh, M. and Kadkhodayan, M. (2017), "Three-dimensional thermo-elastic analysis and dynamic response of a multi-directional functionally graded skew plate on elastic foundation", *Compos. Part B: Eng.*, **125**, 227-240.

Almeyda, E.Y., Montes, C.H., Ramos, R.R., Díaz, G.R., Realpozo, L.J.C., Bravo C.J. and Sabina, F.J. (2017), "Influence of imperfect interface and fiber distribution on the antiplane effective magneto-electro-elastic properties for fiber reinforced composites", *Int. J. Solids Struct.*, **112**, 155-168.

Ardestani, M.M., Zhang, L.W. and Liew, K.M. (2017), "Isogeometric analysis of the effect of CNT orientation on the static and vibration behaviors of CNT-reinforced skew composite plates", *Comput. Method. Appl. M.*, **317**, 341-379.

Barandiaran, J.M., Kurlyandskaya, G.V., de Cos, D., García-Arribas, A. and Vas'kovskiy, V.O. (2009), "Multilayer magnetoimpedance sensor for nondestructive testing", *Sensor Lett.*, **7**, 374-377.

Bagheri, R., Ayatollahi, M. and Mousavi, S.M. (2017), "Stress analysis of a functionally graded magneto-electro-elastic strip with multiple moving cracks", *Math. Mech. Solids*, **22**(3), 304-323.

Bhangale, R.K. and Ganesan, N. (2005), "Free vibration studies of simply supported nonhomogeneous functionally graded magneto-electro-elastic finite cylindrical shells", *J. Sound Vib.*, **288**, 412-422.

Bhangale, R.K. and Ganesan, N. (2006), "Free vibration of simply supported functionally graded and layered magneto-electro-elastic plates by finite element method", *J. Sound Vib.*, **294**, 1016-1038.

Boomgaard, V.J. and Born, R.A. (1978), "Sintered magnetoelectric composite material $BaTiO_3$-Ni (Co, Mn)Fe_2O_4", *J. Mater. Sci.*, **13**(7), 1538-1548.

Buchanan, G.R. (2004), "Layered versus multiphase magneto-electro-elastic composites", *Compos. Part B: Eng.*, **35**(5), 413-420.

Chen, J.Y., Heyliger, P.R. and Pan, E. (2014), "Free vibration of three-dimensional multilayered magneto-electro-elastic plates under clamped/free boundary conditions", *J. Sound Vib.*, **333**, 4017-4029.

Chen, J., Guo, J. and Pan, E. (2017), "Wave propagation in magneto-electro-elastic multilayered plates with nonlocal effect", *J. Sound Vib.*, **400**, 550-563.

Ebrahimi, F., Naei, M.H. and Rastgoo, A. (2009), "Geometrically nonlinear vibration analysis of piezoelectrically actuated FGM plate with an initial large deformation", *J. Mech. Sci. Technol.* **23**(8), 2107-2124.

Ebrahimi, F. and Rastgoo, A. (2011), "Nonlinear vibration analysis of piezo-thermo-electrically actuated functionally graded circular plates", *Arch. Appl. Mech.*, **81**(3), 361-383.

Ebrahimi, F. and Rastgoo, A. (2009), "Nonlinear vibration of smart circular functionally graded plates coupled with piezoelectric layers", *Int. J. Mech. Mater. Des.*, **5**(2), 157-165.

Ebrahimi, F., Jafari, A. and Barati, M.R. (2017), "Vibration analysis of magneto-electro-elastic heterogeneous porous material plates resting on elastic foundations", *Thin-Wall. Struct.*, **119**, 33-46.

Ebrahimi, F. and Barati, M.R., (2016), "Buckling analysis of piezoelectrically actuated smart nanoscale plates subjected to magnetic field", *J. Intel. Mat. Syst. Str.*, **28**, 1472-1490.

Ebrahimi, F. and Dabbagh, A. (2017), "On flexural wave propagation responses of smart FG magneto-electro-elastic nanoplates via nonlocal strain gradient theory", *Compos. Struct.*, **162**, 281-293.

Feng, W. and Liu, J. (2007), "Dynamic analysis of a magneto-electro-elastic material with a semi-infinite mode-III crack under point impact loads", *Struct. Eng. Mech.*, **27**(5), 609-623.

García-Macías, E., Castro-Triguero, R., Flores, E.I.S., Friswell, M.I. and Gallego, R. (2016), "Static and free vibration analysis of functionally graded carbon nanotube reinforced skew plates", *Compos. Struct.*, **140**, 473-490.

Garg, A.K., Khare, R.K. and Kant, T. (2006), "Free vibration of skew fiber-reinforced composite and sandwich laminates using a shear deformable finite element model", *J. Sand. Struct. Mater.*, **8**, 33-53.

Guan, Q. (2012), "The free vibration of the Magneto-electro-elastic materials laminated circular plate", *Adv. Mater. Res.*, **374**, 2193-2199.

Jamalpoor, A., Ahmadi-Savadkoohi, A., Hossein, M. and Hosseini-Hashemi, S. (2017), "Free vibration and biaxial buckling analysis of double magneto-electro-elastic nanoplate-systems coupled by a visco-Pasternak medium via nonlocal elasticity theory", *Eur. J. Mech. A-Solid.*, **63**, 84-98.

Jiang, A. and Ding, H.J. (2004), "Analytical solutions to magneto-electro-elastic beams", *Struct. Eng. Mech.*, **18**(2), 195-209.

Jiang, A. and Ding, H.J. (2005), "Green's functions and boundary element method for a magneto-electro-elastic half-plane", *Struct. Eng. Mech.*, **20**(2), 259-264.

Jiang, A. and Ding, H.J. (2007), "Analytical solutions for density functionally gradient magneto-electro-elastic cantilever beams", *Smart Struct. Syst.*, **3**(2), 173-188.

Kanasogi, R.M. and Ray, M.C. (2013), "Active constrained layer damping of smart skew laminated composite plates using 1-3 piezoelectric composites", *J. Compos.*, Hindawi Publishing Corporation. http://dx.doi.org/10.1155/2013/824163

Kattimani, S.C. and Ray, M.C. (2014a), "Smart damping of geometrically nonlinear vibrations of magneto-electro-elastic plates", *Compos. Struct.*, **114**, 51-63.

Kattimani, S.C. and Ray, M.C. (2014b), "Active control of large amplitude vibrations of smart magneto-electro-elastic doubly curved shells", *Int. J. Mech. Mater. Des.*, **10**, 351-378.

Kattimani, S.C. and Ray, M.C. (2015), "Control of geometrically nonlinear vibrations of functionally graded Magneto-electro-elastic plates", *Int. J. Mech. Sci.*, **99**, 154-167.

Kattimani, S.C. (2017), "Geometrically nonlinear vibration analysis of multiferroic composite plates and shells", *Compos. Struct.*, **163**, 185-194.

Kiani, Y. (2016), "Free vibration of FG-CNT reinforced composite skew plates", *Aerosp. Sci. Technol.*, **58**, 178-188.

Kiran, M.C. and Kattimani, S.C. (2017), "Buckling characteristics and static studies of multilayered magneto-electro-elastic plate", *Struct. Eng. Mech.*, **64**(6), 452-4785.

Kiran, M.C. and Kattimani, S.C. (2018a), "Buckling analysis of skew magneto-electro-elastic plates under in-plane loading", *J. Intel. Mat. Syst. Str.*, **29**(6), 1-17.

Kiran, M.C., Kattimani, S.C. and Vinyas, M. (2018b), "Porosity influence on structural behaviour of skew functionally graded magneto-electro-elastic plate", *Compos. Struct.*, **191**(6), 36-77.

Kondaiah, P., Shankar, K. and Ganesan, N. (2015), "Pyroeffects on magneto-electro-elastic sensor bonded on mild steel cylindrical shell", *Smart Struct. Syst.*, **16**(3), 537-554.

Kondaiah, P. and Shankar, K. (2017), "Pyroeffects on Magneto-Electro-Elastic Sensor patch subjected to thermal load", *Smart Struct. Syst.*, **19**(3), 299-307.

Koma, Y.A. and Zimcik, D.G. (2003), "Applications of smart structures to aircraft for performance enhancement", *Can. Aeronaut. Space J.*, **49**(4), 163-172.

Kumar, R., Mondal, S., Guchhait, S. and Jamatia, R. (2017), "Analytical approach for dynamic instability analysis of functionally graded skew plate under periodic axial compression", *Int. J. Mech. Sci.*, **130**, 41-51.

Kurlyandskaya, G.V., de Cos, D. and Volchkov S.O. (2009), "Magnetosensitive transducers for nondestructive testing

operating on the basis of the giant magnetoimpedance effect: a review", *Russ. J. Nondestr. Test.*, **45**, 377-398.
Lage, R.G., Soares, C.M.M., Soares, C.A.M. and Reddy, J.N. (2004), "Layerwise partial mixed finite element analysis of magneto-electro-elastic plates", *Comput. Struct.*, **82**, 1293-1301.
Liu, J., Zhang, P., Lin, G., Wang, W. and Lu, S. (2016), "Solutions for the magneto-electro-elastic plate using the scaled boundary finite element method", *Eng. Anal. Bound. Elem.*, **68**, 103-114.
Li, X.Y., Ding, H.J. and Chen, W.Q. (2008), "Three-dimensional analytical solution for functionally graded magneto–electro-elastic circular plates subjected to uniform load", *Compos. Struct.*, **83**(4), 381-390.
Li, X.Y., Zheng, R.F., Chen, W.Q., Kang, G.Z., Gao, C.F. and Müller, R. (2017), "Three-dimensional exact magneto-electro-elastic field in an infinite transversely isotropic space with an elliptical crack under uniform loads: Shear mode", *Int. J. Eng. Sci.*, **116**, 104-129.
Miyamoto, Y., Kaysser, W., Rabin, B., Kawasaki, A. and Ford, R.G. (2013), "Functionally graded materials: Design, processing and applications", *Springer Sci. Busi. Media*, 5.
Milazzo, A (2014a), "Refined equivalent single layer formulations and finite elements for smart laminates free vibrations", *Compos. Part B: Eng.*, **61**, 238-253.
Milazzo, A. (2014b), "Large deflection of magneto-electro-elastic laminated plates", *Appl. Math. Model.*, **38**(5), 1737-1752.
Milazzo, A. (2016), "Unified formulation for a family of advanced finite elements for smart multilayered plates", *Mech. Adv. Mater. Struct.*, **23**(9), 971-980.
Mortensen, A. and Suresh, S. (1995), "Functionally graded metals and metal-ceramic composites: Part 1 Processing", *Int. Mater. Rev.*, **40**(6), 239-265.
Moita Simoes, J.M., Mota Soares, C.M. and Mota Soares, C.A. (2009), "Analyses of Magneto-electro-elastic plates using a higher order finite element model", *Compos. Struct.*, **91**, 421-426.
Nan, C.W., Bichurin, M.I., Dong, S., Viehland, D. and Srinivasan, G. (2008), "Multiferroic magnetoelectric composites: Historical perspective, status, and future directions", *J. Appl. Phys.*, **103**(3).
Pan, E. (2001), "Exact solution for simply supported and multilayered magneto-electroelastic plates", *J. Appl. Mech.-T.*, **68**, 608-618.
Pan, E. and Heyliger, P.R. (2002), "Free vibration of simply supported and multilayered magnetoelectro-elastic plates", *J. Sound Vib.*, **252**(3), 429-442.
Pan, E. and Heyliger, P.R. (2003), "Exact solutions for magneto-electro-elastic laminates in cylindrical bending", *Int. J. Solids Struct.*, **40**(24), 6859-6876.
Pan, E. and Han, F. (2005), "Exact solutions for functionally graded and layered magneto-electro-elastic plates", *Int. J. Eng. Sci.*, **43**, 321-339.
Pompe, W., Worch, H., Epple, Friess, M., Gelinsky, M., Greil, P., Hempel, U., Scharnweber, D. and Schulte, K. (2003), "Functionally graded materials for biomedical applications", *Mater. Sci. Eng.: A*, **362**(1), 40-60.
Ramirez, F., Heyliger, P.R. and Pan, E. (2006), "Free vibration response of two-dimensional magneto-electro-elastic plates", *J. Sound Vib.*, **292**, 626-644.
Ray, M.C., Rao, K.M. and Samanta, B. (1992), "Exact analysis of coupled electroelastic behavior of a piezoelectric plate under cylindrical bending", *Comput. Struct.*, **45**(4), 667-677.
Ray, M.C., Oh, J. and Baz, A. (2001), "Active constrained layer damping of thin cylindrical shells", *J. Sound Vib.*, **240**(5), 921-935.
Ruan, M. and Wang, Z.M. (2016), "Transverse vibrations of moving skew plates made of functionally graded material", *J. Vib. Control.*, **22**(16), 3504-3517.
Shenas, A.G. and Malekzadeh, P. (2016), "Free vibration of functionally graded quadrilateral microplates in thermal environment", *Thin-Wall. Struct.*, **106**, 294-315.
Shooshtari, A. and Razavi, S. (2017), "Vibration of a multiphase magneto-electro-elastic simply supported rectangular plate subjected to harmonic forces", *J. Intel. Mat. Syst. Str.*, **28**(4), 451-467.
Vinyas, M. and Kattimani, S.C. (2017a), "A Finite element based assessment of static behavior of multiphase magneto-electro-elastic beams under different thermal loading", *Struct. Eng. Mech.*, **62**(5), 519-535.
Vinyas, M. and Kattimani S.C. (2017b), "Static studies of stepped functionally graded magneto-electro-elastic beam subjected to different thermal loads", *Compos. Struct.*, **163**, 216-237.
Wang, H.M. and Ding, H.J. (2006), "Spherically symmetric transient responses of functionally graded magneto-electro-elastic hollow sphere", *Struct. Eng. Mech.*, **23**(5), 525-542.
Waksmanski, N. and Pan, E. (2016), "An analytical three-dimensional solution for free vibration of a magneto-electro-elastic plate considering the nonlocal effect", *J. Intel. Mat. Syst. Str.*, **28**, 1501-1513.
Wang, J., Chen, L. and Fang, S. (2003), "State vector approach to analysis of multilayered magneto- electro-elastic plates", *Int. J. Solids Struct.*, **40**, 1669-1680.
Wang, Y., Xu, R. and Ding, H. (2011), "Axisymmetric bending of functionally graded circular magneto-electro-elastic plates", *Eur. J. Mech. A Solid*, **30**(6), 999-1011.
Xiao, D., Han, Q., Liu, Y. and Li, C. (2016), "Guided wave propagation in an infinite functionally graded magneto-electro-elastic plate by the Chebyshev spectral element method", *Compos. Struct.*, **153**, 704-711.
Zhang, R., Duan, Y., Or, S.W. and Zhao, Y. (2014), "Smart elasto-magneto-electric (EME) sensors for stress monitoring of steel cables: design theory and experimental validation", *Sensors*, **14**(8), 13644-13660.
Zhou, Y. and Zhu, J. (2016), "Vibration and bending analysis of multiferroic rectangular plates using third-order shear deformation theory", *Compos. Struct.*, **153**, 712-723.

CC

Appendix

The shape functions $[N_t]$, $[N_r]$, $[N_\phi]$ and $[N_\psi]$ appearing in Eq. (14) are given as follows:

$$[N_t]=\begin{bmatrix} N_1 & 0 & 0 & N_2 & 0 & 0 & \dots & N_8 & 0 & 0 \\ 0 & N_1 & 0 & 0 & N_2 & 0 & \dots & 0 & N_8 & 0 \\ 0 & 0 & N_1 & 0 & 0 & N_2 & \dots & 0 & 0 & N_8 \end{bmatrix}^T$$

$$[N_r]=\begin{bmatrix} N_1 & 0 & 0 & 0 & N_2 & 0 & 0 & 0 & \dots & N_8 & 0 & 0 & 0 \\ 0 & N_1 & 0 & 0 & 0 & N_2 & 0 & 0 & \dots & 0 & N_8 & 0 & 0 \\ 0 & 0 & N_1 & 0 & 0 & 0 & N_2 & 0 & \dots & 0 & 0 & N_8 & 0 \\ 0 & 0 & 0 & N_1 & 0 & 0 & 0 & N_2 & \dots & 0 & 0 & 0 & N_8 \end{bmatrix}^T \quad \text{(A1)}$$

$$[N_\phi]=[N_1 \quad N_2 \quad N_3 \quad N_4 \quad N_5 \quad N_6 \quad N_7 \quad N_8]^T$$

$$[N_\psi]=[N_1 \quad N_2 \quad N_3 \quad N_4 \quad N_5 \quad N_6 \quad N_7 \quad N_8]^T$$

The nodal strain-displacement matrices [b_{tb}], [b_{rb}], [b_{ts}] and [b_{rs}] appearing in the Eq. (16) are given by

$$\begin{aligned} [b_{bt}] &= [b_{bt1} \; b_{bt2} \; \dots \; b_{bt8}], \\ [b_{br}] &= [b_{br1} \; b_{br2} \; \dots \; b_{br8}], \\ [b_{st}] &= [b_{st1} \; b_{st2} \; \dots \; b_{st8}] \text{ and} \\ [b_{sr}] &= [b_{sr1} \; b_{sr2} \; \dots \; b_{sr8}] \end{aligned} \quad \text{(A2)}$$

The various sub-matrices [b_{bt}], [b_{br}], [b_{st}] and [b_{sr}] (i = 1, 2, 3, . . ., 8) are as follows

$$[b_{bt}]=\begin{bmatrix} \frac{\partial N_i}{\partial x} & 0 & 0 \\ 0 & \frac{\partial N_i}{\partial y} & 0 \\ \frac{\partial N_i}{\partial y} & \frac{\partial N_i}{\partial x} & 0 \end{bmatrix}; [b_{st}]=\begin{bmatrix} 0 & 0 & \frac{\partial N_i}{\partial x} \\ 0 & 0 & \frac{\partial N_i}{\partial y} \end{bmatrix};$$

$$[b_{br}]=\begin{bmatrix} \frac{\partial N_i}{\partial x} & 0 & 0 & 0 \\ 0 & \frac{\partial N_i}{\partial y} & 0 & 0 \\ \frac{\partial N_i}{\partial y} & \frac{\partial N_i}{\partial x} & 0 & 0 \\ 0 & 0 & N_i & 0 \\ 0 & 0 & 0 & N_i \end{bmatrix}; [b_{sr}]=\begin{bmatrix} N_i & 0 & 0 & 0 \\ 0 & N_i & 0 & 0 \\ 0 & 0 & \frac{\partial N_i}{\partial x} & 0 \\ 0 & 0 & \frac{\partial N_i}{\partial y} & 0 \\ 0 & 0 & 0 & \frac{\partial N_i}{\partial x} \\ 0 & 0 & 0 & \frac{\partial N_i}{\partial y} \end{bmatrix} \quad \text{(A3)}$$